AFOSR·TR· 89-0054

②

AD-A203 732

CHARACTERIZATION OF PARTICLE COMBUSTION IN A RIJKE BURNER

by

M.W. Beckstead

Brigham Young University

Provo, UT 84602

November 1988

89 2 8 034

REPORT DOCUMENTATION PAGE

Form Approved
OMB No. 0704-0188

1a. REPORT SECURITY CLASSIFICATION Unclassified	1b. RESTRICTIVE MARKINGS
2a. SECURITY CLASSIFICATION AUTHORITY	3. DISTRIBUTION / AVAILABILITY OF REPORT Approved for public release; distribution is unlimited
2b. DECLASSIFICATION / DOWNGRADING SCHEDULE	

4. PERFORMING ORGANIZATION REPORT NUMBER(S)	5. MONITORING ORGANIZATION REPORT NUMBER(S) AFOSR-TR- 89-0054

6a. NAME OF PERFORMING ORGANIZATION Brigham Young University	6b. OFFICE SYMBOL (If applicable)	7a. NAME OF MONITORING ORGANIZATION AFOSR/NA
6c. ADDRESS (City, State, and ZIP Code) Department of Chemical Engineering Provo, UT 84602		7b. ADDRESS (City, State, and ZIP Code) Building 410, Bolling AFB DC 20332-6448

8a. NAME OF FUNDING / SPONSORING ORGANIZATION AFOSR/NA	8b. OFFICE SYMBOL (If applicable) NA	9. PROCUREMENT INSTRUMENT IDENTIFICATION NUMBER AFOSR-83-0157

8c. ADDRESS (City, State, and ZIP Code) Building 410, Bolling AFB DC 20332-6448	10. SOURCE OF FUNDING NUMBERS			
	PROGRAM ELEMENT NO. 61102F	PROJECT NO. 2308	TASK NO. A1	WORK UNIT ACCESSION NO.

11. TITLE (Include Security Classification)
(U) Characterization of Particle Combustion in a Rijke Burner

12. PERSONAL AUTHOR(S)
M.W. Beckstead

13a. TYPE OF REPORT Final	13b. TIME COVERED FROM March 83 to Sept 88	14. DATE OF REPORT (Year, Month, Day) 88 November 29	15. PAGE COUNT 63

16. SUPPLEMENTARY NOTATION

17.	COSATI CODES		18. SUBJECT TERMS (Continue on reverse if necessary and identify by block number)
FIELD	GROUP	SUB-GROUP	Unstable Combustion, Distributed Combustion, Acoustic Instability.

19. ABSTRACT (Continue on reverse if necessary and identify by block number)

This report summarizes a research program to study the acoustic interaction of particle additives used in solid propellants. Various examples of combustion instability found in the literature are discussed that give evidence to the existence and nature of distributed combustion. A modified Rijke burner was constructed as the basic experimental tool and was characterized extensively. Stability boundaries were determined, and growth rates were observed to increase with increasing oxygen content and overall mass flow rate. The data indicate that the overall acoustic driving forces in a Rijke burner are dependent upon the acoustic mode shape relative to the flame location and the distribution of energy through the burner, (i.e. the gas flow rates and heat losses). A mathematical model for the Rijke burner has been developed which accounts for the effects of heat loss, variable gas temperature, and particle interactions on acoustic oscillations. The model has been verified by comparing predicted frequency and growth rates for several simple test cases with the corresponding analytical solutions. The model was also compared directly with the experimental data.

20. DISTRIBUTION / AVAILABILITY OF ABSTRACT ☒ UNCLASSIFIED/UNLIMITED ☒ SAME AS RPT. ☒ DTIC USERS	21. ABSTRACT SECURITY CLASSIFICATION Unclassified	
22a. NAME OF RESPONSIBLE INDIVIDUAL Dr Mitat Birkan	22b. TELEPHONE (Include Area Code) (202) 767-4935	22c. OFFICE SYMBOL AFOSR/NA

DD Form 1473, JUN 86 — Previous editions are obsolete.

TABLE OF CONTENTS

LIST OF FIGURES

LIST OF TABLES

1.0 INTRODUCTION

This report summarizes the work performed on a research program to study the acoustic interaction of particle additives used in solid propellants for performance enhancement and acoustic suppression. A modified Rijke burner which had been constructed previously has been modified extensively to aid in the study.

Acoustic suppressants have been added to low smoke and smokeless propellants for the past decade. For many years aluminum was a panacea for combustion instability. However, as the motivation to eliminate smoke in rocket exhausts increased, aluminum began to be eliminated from propellant formations. In an attempt to avoid combustion instability, ingredients were sought that would act as acoustic suppressants. For the past decade, the suppressants most often used in tactical motors have been ZrC and graphite flake. The rationale for using these additives was based on particle damping theory which in turn is based on energy dissipation by viscous drag. When ZrC was first added to propellants it was considered to be an "inert" additive. However, data obtained during the past few years in the Rijke burner show that ZrC is burning. This phenomenon of the acoustic interaction of burning particles has been referred to as 'distributed combustion'.

Past mathematical models for the Rijke tube did not consider heat loss or particle effects, both important in the Rijke burner. As a result, previous Rijke tube models are inadequate for modelling the Rijke burner. A new numerical model for the Rijke burner has been developed to account for the effects of varying temperature (heat loss) and particles. The objective of this model is prediction of characteristic frequencies and growth rates for oscillations in a Rijke burner. The model has been compared to several analytical test cases and gives good results, typically within 1% for frequency and 6% for growth rate.

The first section of the report discussed various examples found in the literature that give evidence to the existence and nature of distributed combustion. The basic approach used with the Rijke burner is then discussed, followed by a brief description of the mathematical model. Then the results from the model are compared with the experimental data.

1

2.0 GENERAL EVIDENCE FOR DISTRIBUTED COMBUSTION

2.1 INTRODUCTION

Distributed combustion refers to a burning particle which reacts far from the burning surface, exchanging energy with an acoustic environment. This process of distributed combustion has generally been ignored in acoustic analyses of rocket motors in the past. It is normally assumed that a particle additive (usually aluminum) burns close enough to the propellant surface to be treated as a boundary condition. This section of the report presents a number of examples of experimental data, general observations and theoretical calculations, which provide evidence that burning particles can and do burn far from the propellant surface and can have a strong interaction with the acoustics of a system. None of the examples are completely quantitative. However, when one considers the several examples together, the evidence seems to indicate that distributed combustion is a significant effect that should not be neglected.

2.2 VELOCITY COUPLED T-BURNER EXAMPLES

The velocity coupled T-burner (VCTB) consists of a variable area T-burner modified to burn four propellant samples[1]. A small amount of driver sample is located at each end of the T-burner as in a conventional pressure coupled test. These two samples provide pressure coupled driving and a continuous flow of hot combustion products throughout the chamber. The test samples are located midway between the vent and the end of the T-burner, resulting in a maximum contribution to first mode velocity coupling driving while minimizing contributions to the second mode of the T-burner. Data are obtained by varying the size of the test sample.

Recently questions have been raised about the concepts of velocity coupling[2,3], and perhaps the quantitative response values of velocity coupling measured in the VCTB are subject to question. However, the qualitative nature of the data and the relative magnitudes of the measured quantities are relevant and can provide valuable insight to the combustion mechanisms that occur in a burner.

Several propellants have been tested[1,4-6] in the VCTB and an examination of the data in general shows some very interesting and significant trends. Most significant, metallized propellants invariably have shown a higher response and greater driving than non-metallized propellants. Second, the "measured", velocity coupled response functions for metallized propellants were typically of order 10 while pressure coupled response functions and velocity coupled response functions for non-metallized propellants were of order 1-2.

Figure 1 shows a comparison of growth rates measured in a VCTB versus those measured in a variable area, pressure-coupled T-Burner for CYH 1-14, a metallized CMDB propellant. It is readily apparent that the VCTB configuration results in much greater driving than the pressure coupled configuration. For the same amount of propellant, growth rates were 50 to 75 sec^{-1} larger. Using conventional techniques to

reduce the data[1], the conclusion was reached that the velocity coupling response was 12, which was much greater than the pressure coupled response value of 2.
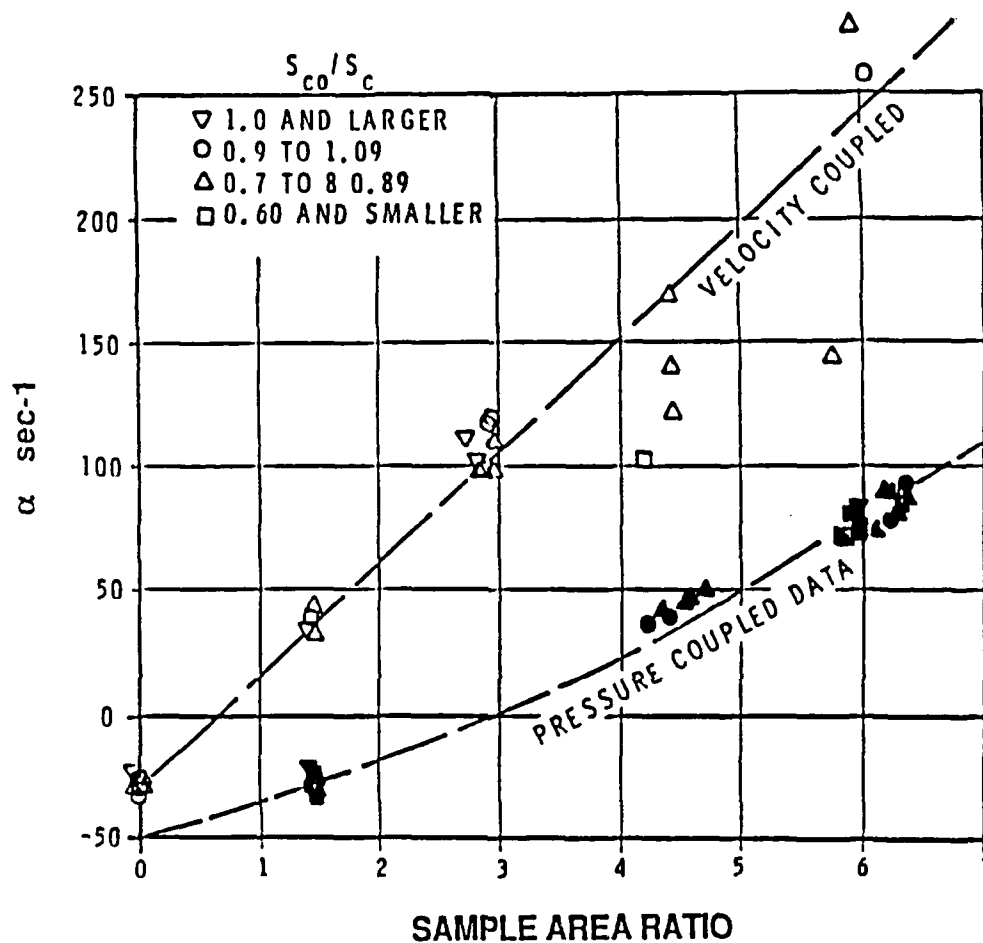
Figure 1. Comparison of data from pressure coupled and velocity coupled T-burner.

Measurements using other propellants showed very similar results. A metallized composite propellant (ANB-3066) yielded a velocity coupled response of ~5 and a pressure coupled response of ~1.5[4]. The measured response functions of a large number of metallized cross linked double base (XLDB) propellants[5] are plotted in Figure 2. Again, the measured velocity coupled response values are a factor of 5-6 greater than the corresponding pressure coupled values. By contrast non-metallized propellants that have been characterized in the VCTB have response functions values comparable to the pressure coupled response functions[4,6] as shown in Figure 3. These non-metallized propellants (both XLDB and HTPB) were tested at several different test conditions. There is no significant difference nor trend between the pressure coupled and velocity coupled data. This is a very dramatic difference. The measured growth rates and corresponding velocity coupled response functions of the metallized propellants are consistently much greater (by a factor of 5 to 6) than either the pressure coupled response or the velocity coupled response of the non-metallized propellants.

3
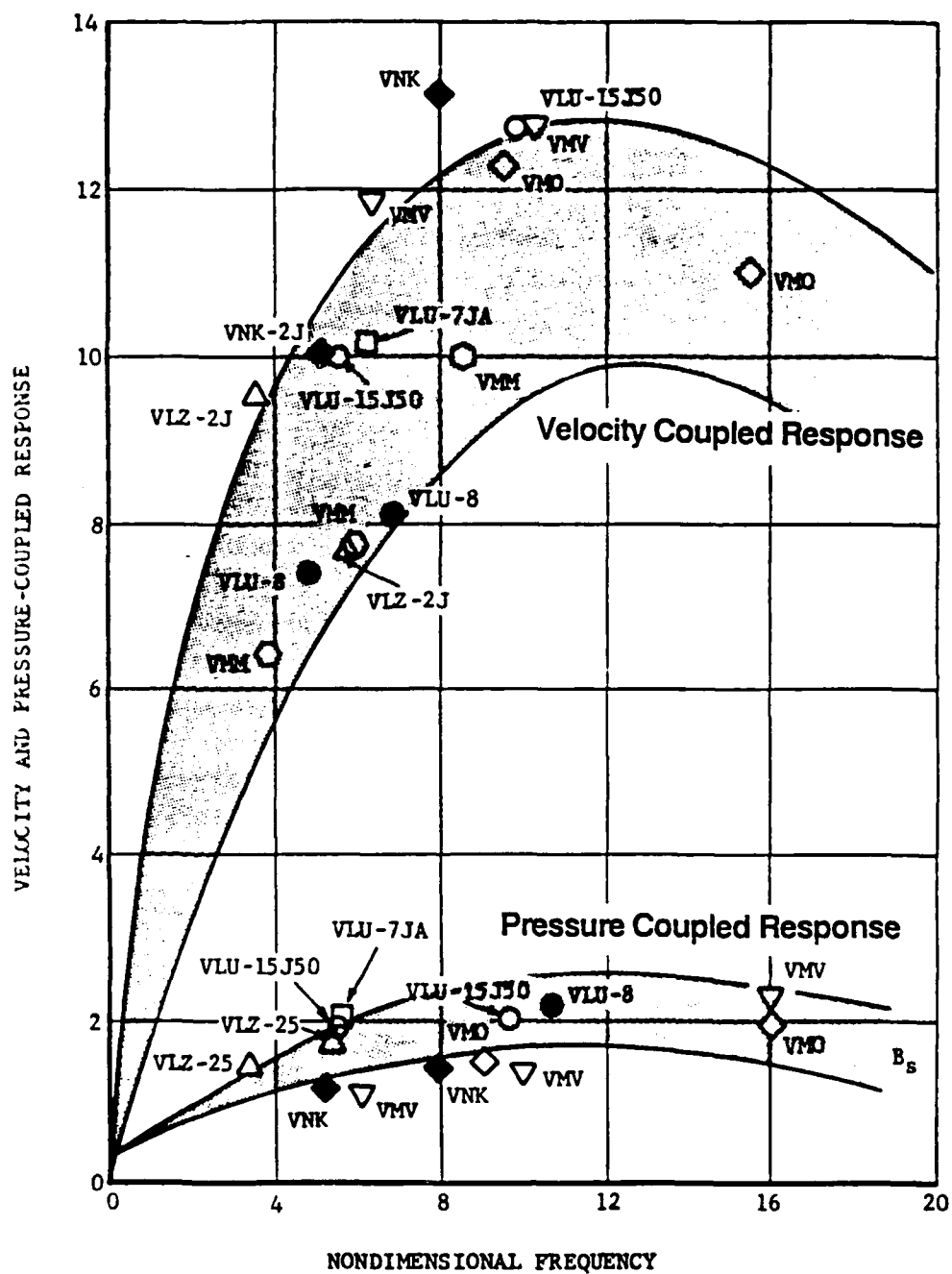
Figure 2. Pressure and velocity coupled response function values for XLDB propellants.
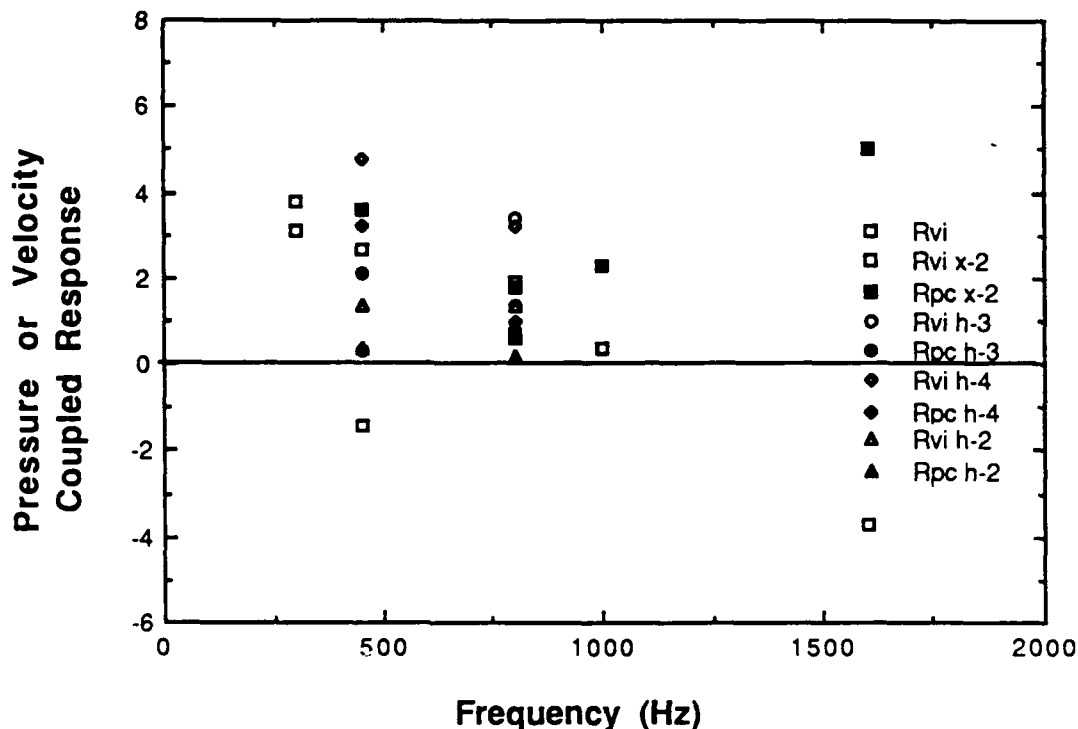
Figure 3. Pressure coupled (solid symbols) and velocity coupled (open symbols) responsed function values for six different nonmetallized propellants, varying pressure and frequency.

The actual mechanism leading to this very significant increase in the propellant response is subject to some conjecture. However, it appears most probable that the responsible mechanism is distributed combustion of the aluminum. It appears that the aluminum is swept from the burning surface and burns in the gas phase at some distance from the surface. This mode of combustion does not fit into the surface response functions concepts which form the basis of the assumptions that lead to pressure and velocity coupled response functions within the normal theoretical description of either a T-burner or rocket motor environment. Therefore, it appears that the measurements made in the VCTB with metallized propellants, are more characteristic of distributed combustion than of velocity coupling. With metallized propellants the VCTB is apparently measuring distributed combustion characteristics.

Another observation that is a discrepancy in the interpretation of VCTB data, is that the measured value of the velocity coupled response varies with the location of the propellant test sample. Using the CYH propellant, the measured velocity coupled response values at locations of L/8, L/4 and 3L/8 are 11, 13, and 16 respectively[4]. Obviously, this is an inconsistency. However, if distributed combustion is occurring one would logically expect the response to change with changing sample location.

One of the most significant discrepancies with interpreting the VCTB has occurred with end vented burners[4,7]. Using the standard interpretation of velocity coupling[8], results obtained from end vented burners lead to inconsistent conclusions.

5

Direct comparison of the VCTB data and end vented data should give a relatively independent measure of the velocity coupled response. However, the results are not consistent with the results obtained directly from the VCTB. Again, distributed combustion effects would cause very different results between a VCTB and an end vented burner due to the very different residence times in the two different configurations.

A fourth observation relevant to the VCTB involves the limiting amplitude reached by the oscillatory pressure. The limiting amplitude is determined by the nonlinearities of the system. A method of reducing data in terms of the growth rate and the limiting amplitude has been presented previously[9,10]. The nonlinear parameter,

$$\Pi_{NL} = \frac{\alpha/f}{\Delta P/P} \tag{1}$$

can be used as a measure of the nonlinearities of the system. Although limiting amplitude data are usually not reported, there are some data available. Figure 4 represents the general trends observed[9,10]. Data for metallized propellants in the VCTB have values approaching 10 while metallized propellants in the pressure coupled T-burner have values of 2-5. Non-metallized propellants in either burner have values less than one (typically ~0.3 to ~0.5). Again the implication is that the metallized propellants in the VCTB are exhibiting a different combustion mechanism than the other propellants and burners.
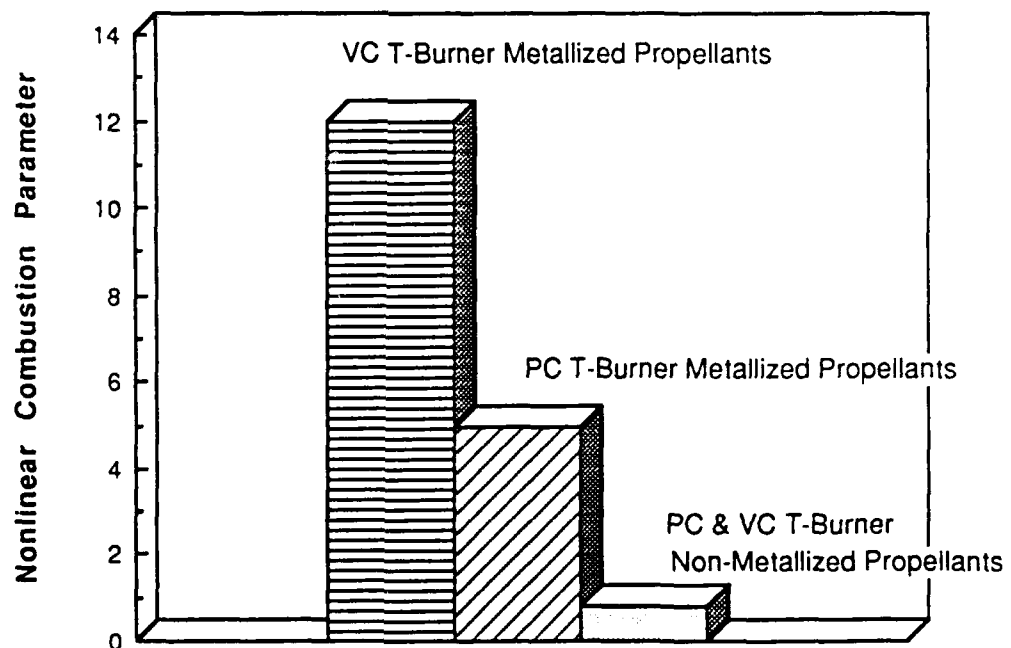
Figure 4. Nonlinear combustion parameter for metallized and nonmetallized propellants in both pressure coupled and velocity coupled T-burners.

2.3 PRESSURE COUPLED T-BURNER DATA

ANB-3066 was the standard propellant used as part of the T-burner workshop program[11-15] that was performed in the early 1970s. It is a typical composite propellant with a moderate burning rate and a relatively high percentage of aluminum. Data obtained from the variable area T-burner[11] indicated a particulate damping level on the order of 75 sec^{-1} for a frequency of 800 Hz and a pressure of 34 MPa (500 psi). However, the pulsed T-burner gave a particle damping value of ~125 sec^{-1}. The discrepancy in the two numbers has not been fully resolved. It is the author's opinion that this discrepancy is due to two factors: 1) the differing propellant orientation, perpendicular to the flow vs parallel to the flow, will influence the size of aluminum agglomerates; and 2) the pulsed T-burner has a very long residence time due to the small amount of propellant used, whereas the variable area T-burner has much shorter residence times leading to a distributed combustion effect.

NWC workers[16] have shown that the same propellant burning in a side orientation versus an end orientation will give different damping results for the same area ratio for metallized propellants. Furthermore, their data indicate that a side oriented sample will give a reduced damping value compared to the end oriented sample. However, their data were for double base propellants which generally have very different agglomerating characteristics from composite propellants. The orientation undoubtedly causes some difference but not all. Comparable tests for non-metallized propellants showed no significant difference due to the orientation.

The second assumption relates to distributed combustion. Calculations have been performed[17] showing that typical agglomerates in typical flow environments can persist throughout a burner (or motor). Parametric calculations show that an aluminum agglomerate typical of a composite solid propellant will not have a sufficiently long residence time for it to be totally consumed within a typical rocket motor cavity. Figure 5 contains such a comparison for ANB-3066 in an 800 Hz T-burner at 3.4 MPa (500 psi) and a propellant burn rate of 0.81 cm/s (0.32 in./s). The figure shows that agglomerates of 80 μm or greater will not burn completely before leaving the cavity for a propellant area ratio of 6 or greater. This means that an aluminum agglomerate can be contributing energy to the acoustic wave continually as it passes through the cavity.
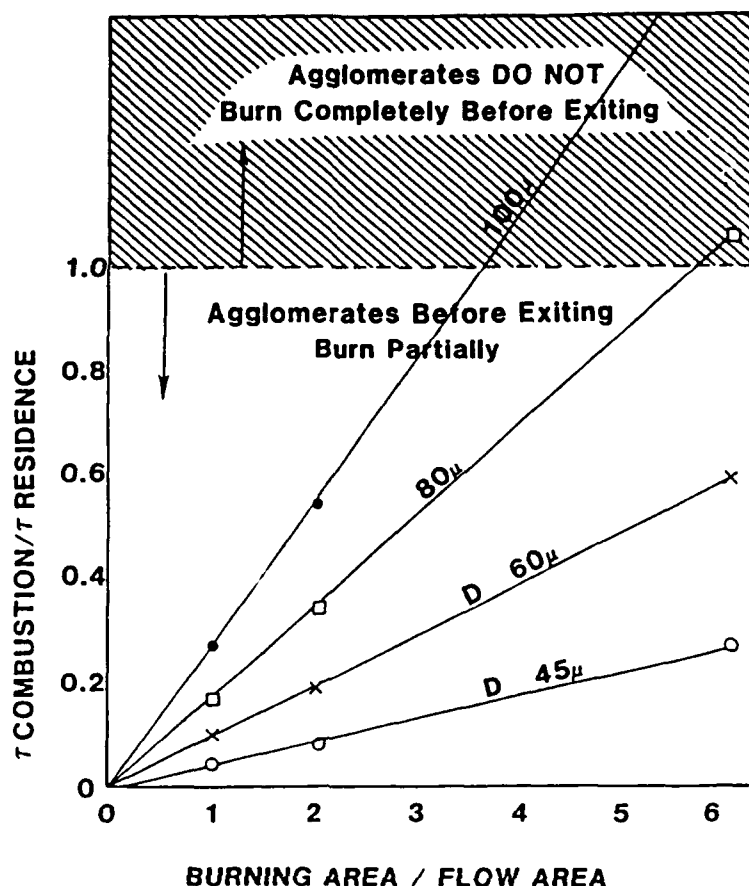
Figure 5.   Comparison of aluminum agglomerate combustion and residence times for an 800 Hz burner at 3.4 MPa (500 psi) and 0.81 cm/sec (0.32 in/sec) varying the relative amount of propellant.

Calculations have been performed[17] to calculate the particle damping simulating the variable area T-burner experiments.   Figure 6 shows the calculated damping coefficient plotted vs the area ratio (i.e., the burning area of propella it divided by the burner cross-sectional area) and four test cases with differing assumed particle distributions.   The four calculated curves are very similar.   Approaching zero propellant in the burner (long residence time), the damping asymptotically approaches a value of ~80 sec^{-1}.   As the amount of propellant increases and the residence time decreases, the damping decreases dramatically approaching limiting values of ~30-40 sec^{-1} at the largest area ratio for which experimental data exists.   The decrease in damping is due to the fact that the aluminum agglomerates are being swept out of the burner without fully burning.   They are sufficiently large that their contribution to the overall damping is negligible.   These calculations indicate that for the assumed particle configurations, the particle damping can change by a factor of at least two. Obviously, the calculations are subject to the accuracy of the assumed particle size distributions.   However, for the four test cases, which cover a fairly wide range of assumed distributions, the final results are very similar. This is an indirect verification that the results are at least qualitatively correct.   Finally, if the aluminum is in fact burning throughout the burner, distributed combustion is occurring.

In another study[18], Wendelken varied the aluminum particle size in a high rate HTPB propellant, holding other formulation variables constant. The T-burner results from that study are shown in Figure 7. The particle damping was essentially constant with varying aluminum size, but did decrease with increased pressure, most likely due to a decrease in the level of agglomeration. Of greater interest is the variation in the combustion growth rate. It varies significantly, passing through a maximum at approximately 12μ, indicating a strong contribution of the aluminum to the combustion driving, i.e. distributed combustion.

	% Aggl.	Capdia (μm)
————	15	12
—·—	45	20
-------	50	18.5
— — —	25	12
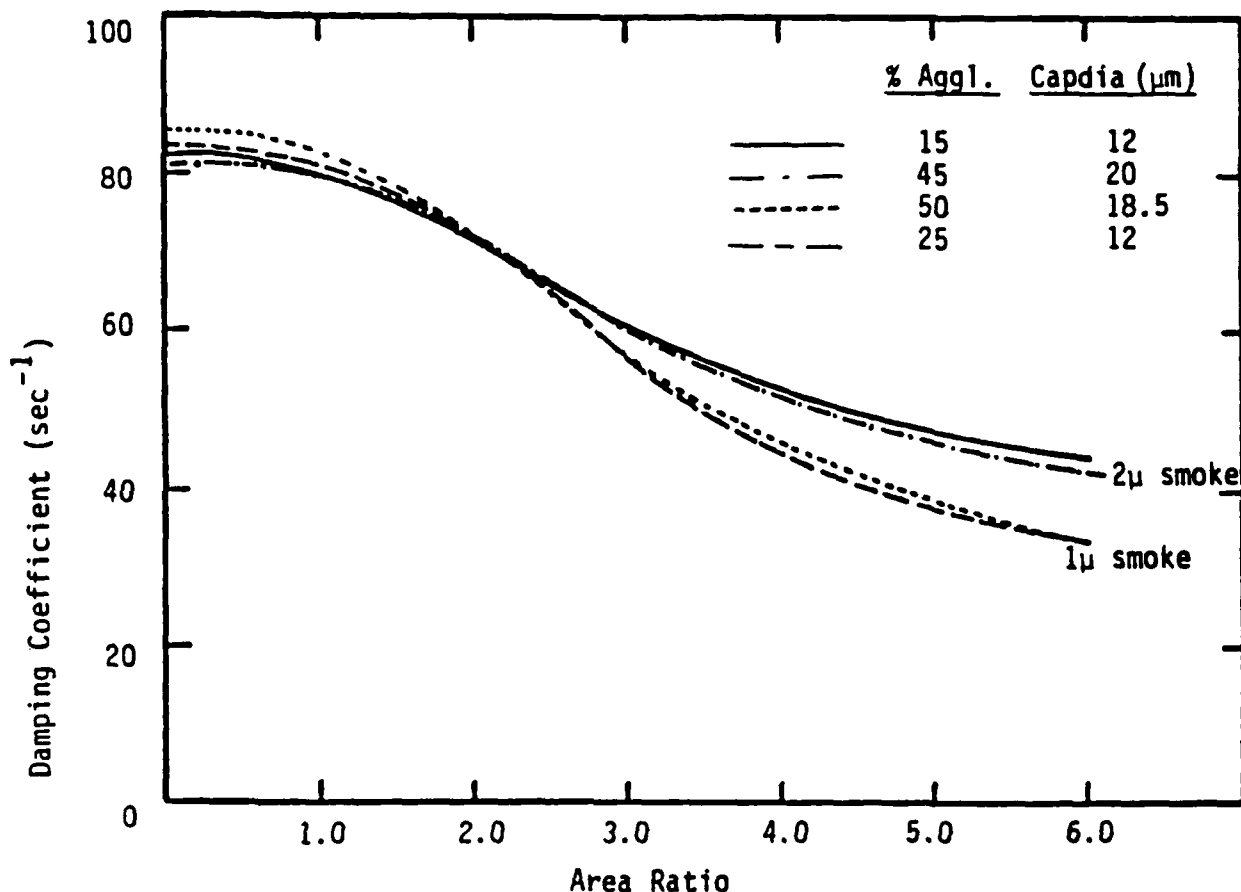
Figure 6.   Calculated damping versus area ratio for 800 Hz test conditions.

FREQ.=650 Hz
ṙ =1.3 IN/SEC @1000 PSIA

⊙ 500 PSIA
△ 1000 PSIA

α_D (SEC-1)

150

100

50

0

0   10   20   30   40   50   60

ALUMINUM PARTICLE SIZE (μ)

α_C (SEC-1)

50

40

30

20

10

0

0   10   20   30   40   50   60

ALUMINUM PARTICLE SIZE (μ)

▣ ANB 3066(REF)
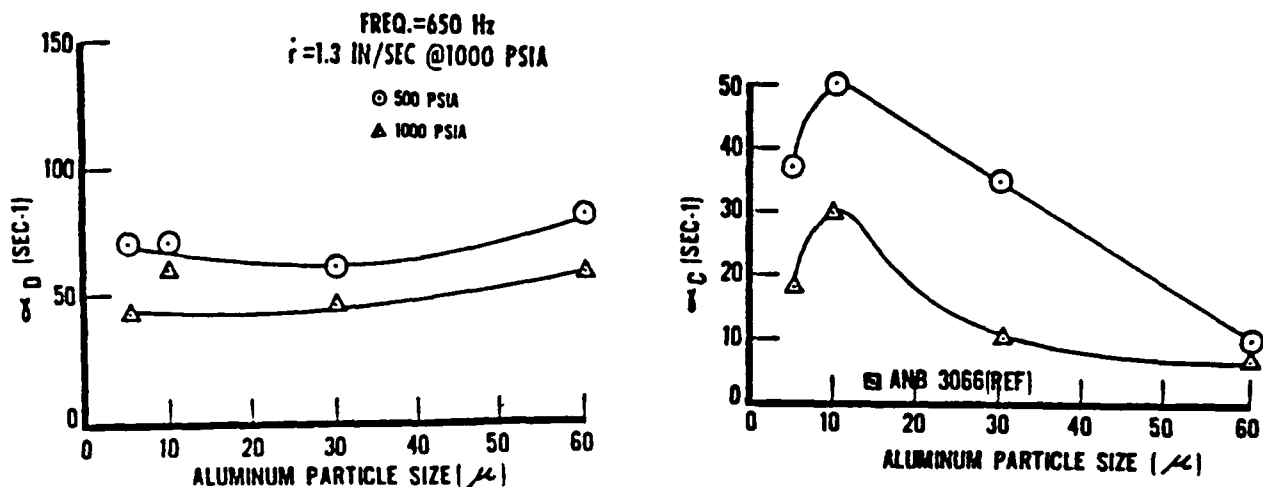
Figure 7.   Combustion driving and damping characteristics of high burn rate HTPB propellant with variable aluminum size.

2.4 LUMINOSITY TESTING

In an earlier study[19] a series of tests were performed in a T-burner with a test sample located in the vicinity of the vent. The original objective of the testing was to test for second mode velocity oscillations which ought to occur near the vent. The test sample luminosity was observed with both a high speed movie camera and a photo diode. The observed results were unanticipated. Typical output from the photo diode is displayed in Figure 8. As the experiment started, the luminosity from the burning sample was intense and saturated the photo diode. However, as the pressure oscillations grew, an amplitude was reached where the luminosity decreased, until there was little or no luminosity. The test results were repeatable and occurred with a variety of metallized propellants, both composite and double base. The high speed movies showed that the burning aluminum was being swept violently from the propellant surface, and the aluminum ultimately was quenched somewhere along the burner, apparently due to the high acoustic velocity stripping the flame from the burning particle. When the driver propellant burned out, the pressure (and velocity) oscillations died down and the aluminum combustion with its associated luminosity re-established itself until the test sample also burned out. During the time period of the minimum luminosity, the test sample continued to regress at its normal burning rate. Apparently, as the acoustic velocity built up, the drag of the burning aluminum was sufficiently great that a large velocity difference developed between the gas and the burning particle. When the velocity difference became great enough, the burning particles were quenched. These experiments show that the aluminum burns a significant distance from the surface and that the burning particles can and are influenced by an acoustic wave. This is another evidence for distributed combustion.
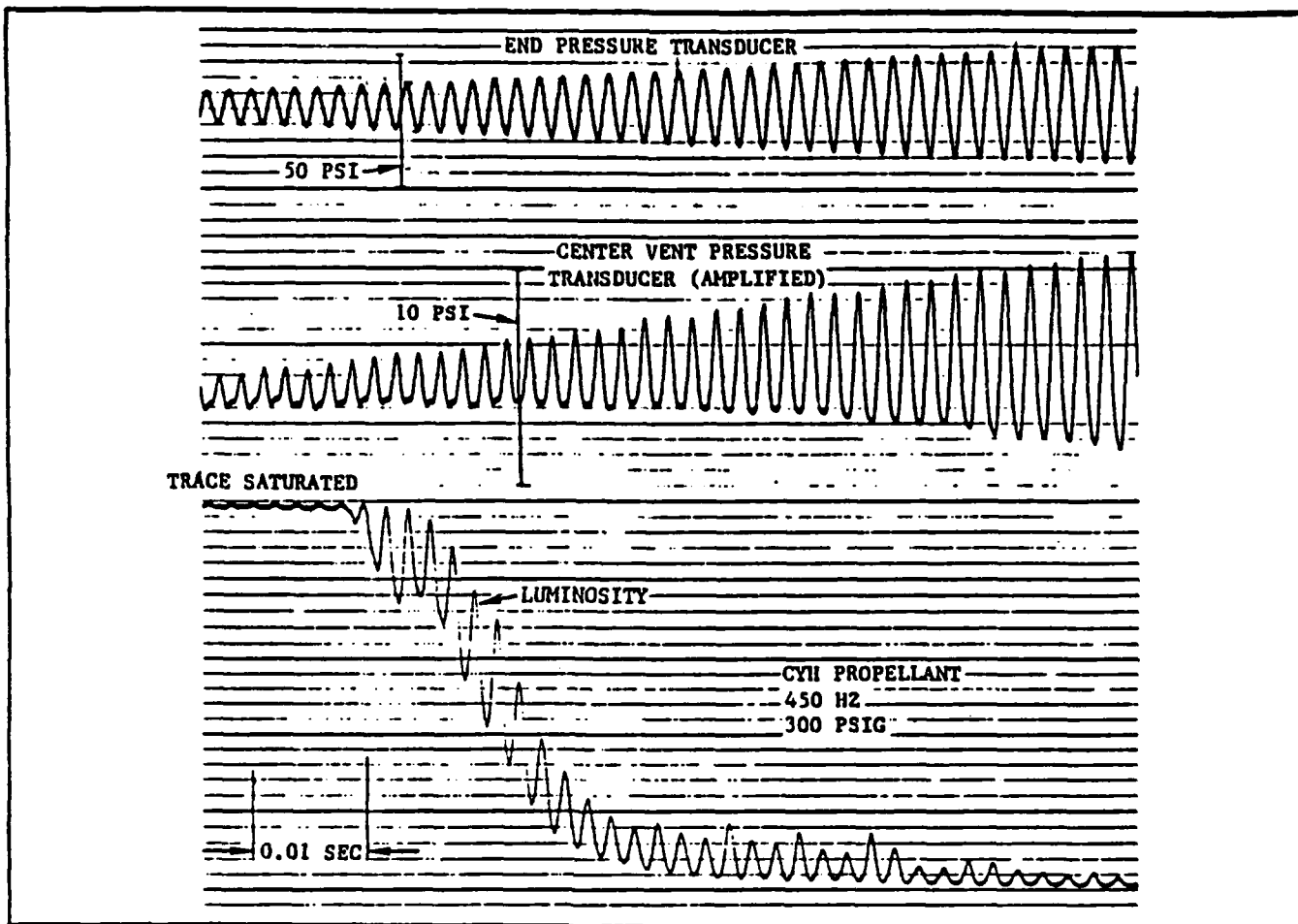
Figure 8. Typical firing with CYH showing the onset of dark combustion mode during high amplitude oscillations.

2.5 RIJKE BURNER RESULTS

Earlier work on the current contract[20] was performed with the gas-fired Rijke burner described in Section 3 with the objective of measuring distributed combustion. Data were obtained in a particle free system and compared to data obtained from tests with varying amounts of aluminum and zirconium carbide. The results are shown in Figure 9. With increasing amounts of either additive, the acoustic driving increased indicating that both additives contributed to the overall system driving, apparently by a distributed combustion mechanism. The increase in driving was as high as 200 sec $^{-1}$ compared to the baseline value (no particles) of 330 sec $^{-1}$. Thus, for these tests the distributed combustion contribution from a small percentage of particles appears to be the same order of magnitude as the driving due to the flame.

11
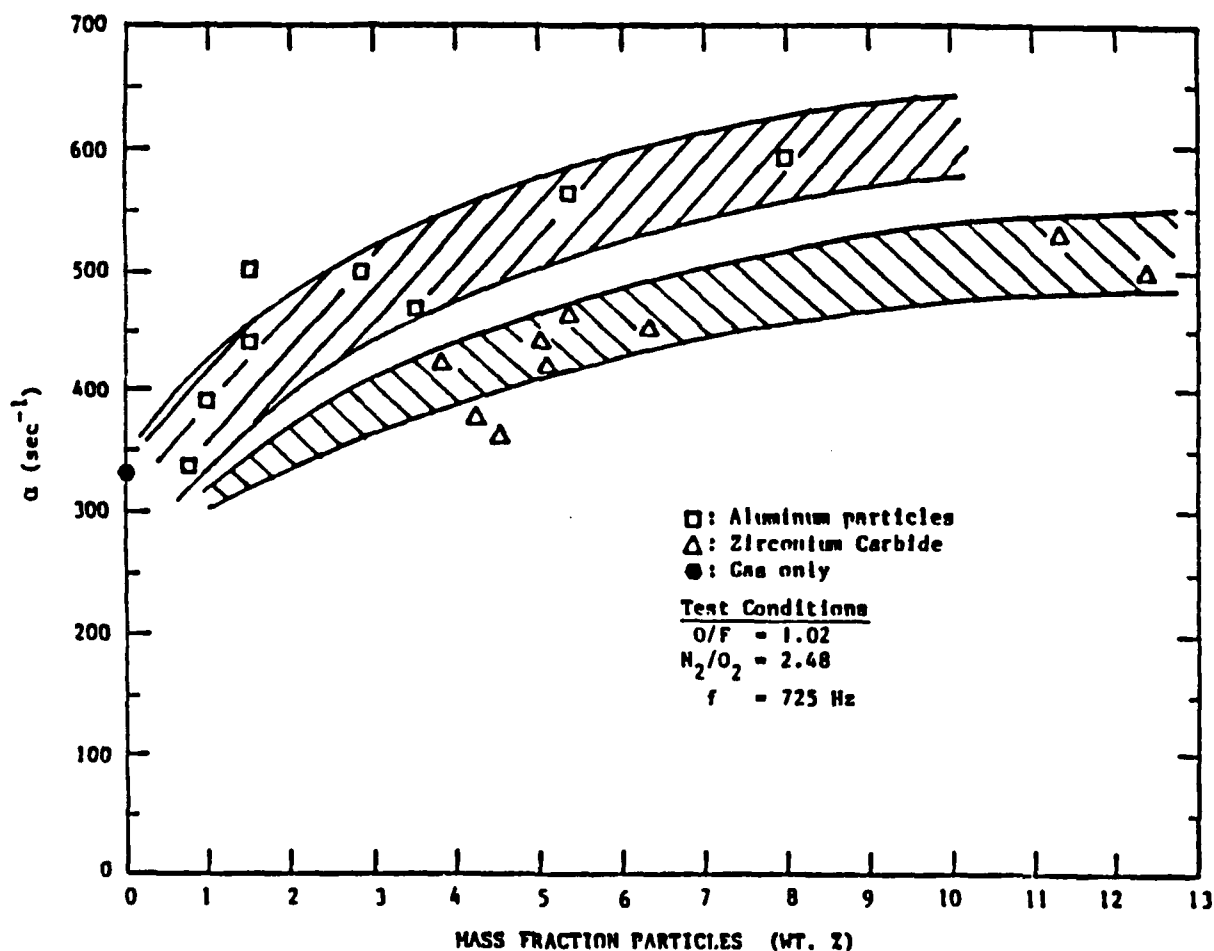
Figure 9. Acoustic growth rate (a) in the Rijke burner vs. mass fraction aluminum and zirconium carbide.

2.6 MOTOR DATA

A few years ago, a high burn rate, high pressure motor experienced acoustic combustion instability[21]. Subsequently, a workshop was held to identify the cause of the instability. Because of the very high burn rate of the propellant and the relatively low frequency of the motor, the pressure coupled response of the propellant was assumed to approach the pressure exponent, and the velocity coupled response was assumed to approach zero. Using these very reasonable assumptions, the SSP code predicted the motor to be stable. After considerable discussion, it was generally agreed that the only driving mechanism, not considered, that could have caused the motor to oscillate was distributed combustion. An initial evaluation of the residence time of aluminum in the motor supports this conclusion due to the very high velocity of the combustion gases. Thus, a very practical application (i.e. a motor) also seems to give evidence of distributed combustion.

2.7 CONCLUSIONS

A variety of sources have been examined for evidence of distributed combustion. Velocity coupled T-burner data indicate response functions of ~10 for metallized propellants, which is much larger than expected. Non-metallized propellants typically have measured response functions of ~1. The large response function is apparently due to distributed combustion of burning metal rather than velocity coupling. In addition, velocity coupled T-burner data give response functions varying with test sample location, which is inconsistent unless the observed effect is due to distributed combustion. Distributed combustion would be expected to give different results depending on sample location or particle residence time, which is observed. Luminosity measurements in a T-burner environment indicate that burning aluminum particles can actually be quenched due to a severe acoustic environment. Attempts have been made to measure velocity coupling using end vented burners, but again, inconsistent answers result. Pulsed/decay T-Burners usually have given different particle damping than variable area T-Burners, but only with metallized propellants. Also, some T-burner data show α_c varying with Al particle size, while α_d remains constant, indicating an effect due to the burning aluminum. Furthermore, specific calculations indicate large burning times for burning Al agglomerates compared to T-burner residence times. These combined results indicate that distributed combustion may well be the cause for many previously unexplained observations of combustion instability.

3.0 CHARACTERIZATION OF THE RIJKE BURNER

3.1 INTRODUCTION

The modified Rijke burner has been developed as a tool to study distributed combustion.[20]   Using the modified Rijke burner has several advantages over T-burners:

1) The burner allows for separation of distributed combustion effects from propellant response effects.
2) Using propane for the fuel eliminates hazardous propellants, which increases operator safety, lowers the cost, and simplifies the experiments.
3) The burner can be operated for extended periods of time (hours) in either an oscillating or non-oscillating configuration, which allows the burner to achieve thermal steady-state in either configuration.

Two significant disadvantages of the modified Rijke burner compared to a T-burner are:

1) The combustion and acoustics interactions may differ significantly at the higher temperatures and pressures found in a rocket motor.
2) *Propane may respond differently than the propellant gases found in a rocket motor.*

These problems could be minimized by operating at higher pressures and burning gases more similar to propellant gases.

In order to validate the theoretical model previously discussed in Section 4[2] and to better understand distributed combustion data from the modified Rijke burner, the burner was characterized without the addition of particles. It must be understood how the various parameters, such as frequency, flame position, length, inlet gas compositions (O_2, N_2, C_3H_8), and energy balance, can affect the acoustic growth rate. This section will discuss the following parameters:

1) Fundamental acoustic principles involved in understanding the thermoacoustic response of the modified Rijke burner,
2) The experimental procedures, including design modifications of the burner and data reduction, and
3) Characterization of the burner with respect to burner orientation, gas flow rates, length, and heat transfer.

3.2 ACOUSTICS

Two criterion for thermoacoustic driving are[23]:

1) An inductive relationship between acoustic pressure and velocity must exist with the velocity leading pressure by 90°, and
2) The product of acoustic velocity and pressure amplitudes must be positive.

The acoustic pressure and velocity mode shapes which satisfy the criterion for acoustic driving for the closed-open boundary conditions[23,24], corresponding to the modified Rijke burner, are shown in Figure 10. In general, the velocity leads the pressure by 90°, and in the gray regions the product of velocity and pressure is positive. The flame locations for maximum acoustic driving are in the center of the gray regions. As is shown in Figure 10, for the closed-open burner used in this study, the fundamental frequency will not drive acoustically. The first mode drives near the center of the tube, the second mode has two regions of driving, the third mode has three regions, etc. Note that because the driving regions of different modes overlap, it is possible for more than one mode to be driving at the same flame location.

The classical Rijke oscillation occurs when an open-open tube is heated with a hot wire gauze in the lower half of the tube. This configuration has a much lower energy input than a burner and generally oscillates in the fundamental or first acoustic mode[25]. Since higher frequencies are more susceptible to energy losses[26], they require more energy to drive them. The modified Rijke burner at Brigham Young University uses a propane flame stabilized on a wire gauze to drive the thermoacoustic standing wave. It is generally operated with a total flame energy input of approximately 4000 cal/min and oscillates in the 400 - 1700 Hz frequency range depending on the tube length. It is possible to minimize multiple acoustic modes by using shorter lengths of tubing and operating in the first or second acoustic mode.

Placing the flame holder in the geometric center of the burner does not necessarily place the flame in the acoustic center because the speed of sound is a function of the temperature and composition. At the higher temperature in the hot end, the speed of sound is faster, making the hot end acoustically shorter and therefore raising the frequency. In addition the temperature in the hot end is not constant, but varies due to heat losses to the burner walls. Section 4 of the report discusses the model used to calculate the acoustic mode shape of the standing wave in the burner with varying gas temperatures.

Previous workers[27,28] found that particles modify the flame acoustical interactions affecting both the steady-state and transient response. Specifically, Braithewaite found that the driving was proportional to the heat of combustion of the additive[28]. In continuing the work of Braithwaite and Gordon[20,28], the experimental apparatus and data acquisition system have been modified and improved significantly. The following sections describe the major design changes made in the modified Rijke burner and its characterization.

15

Driving Positions for Different Modes
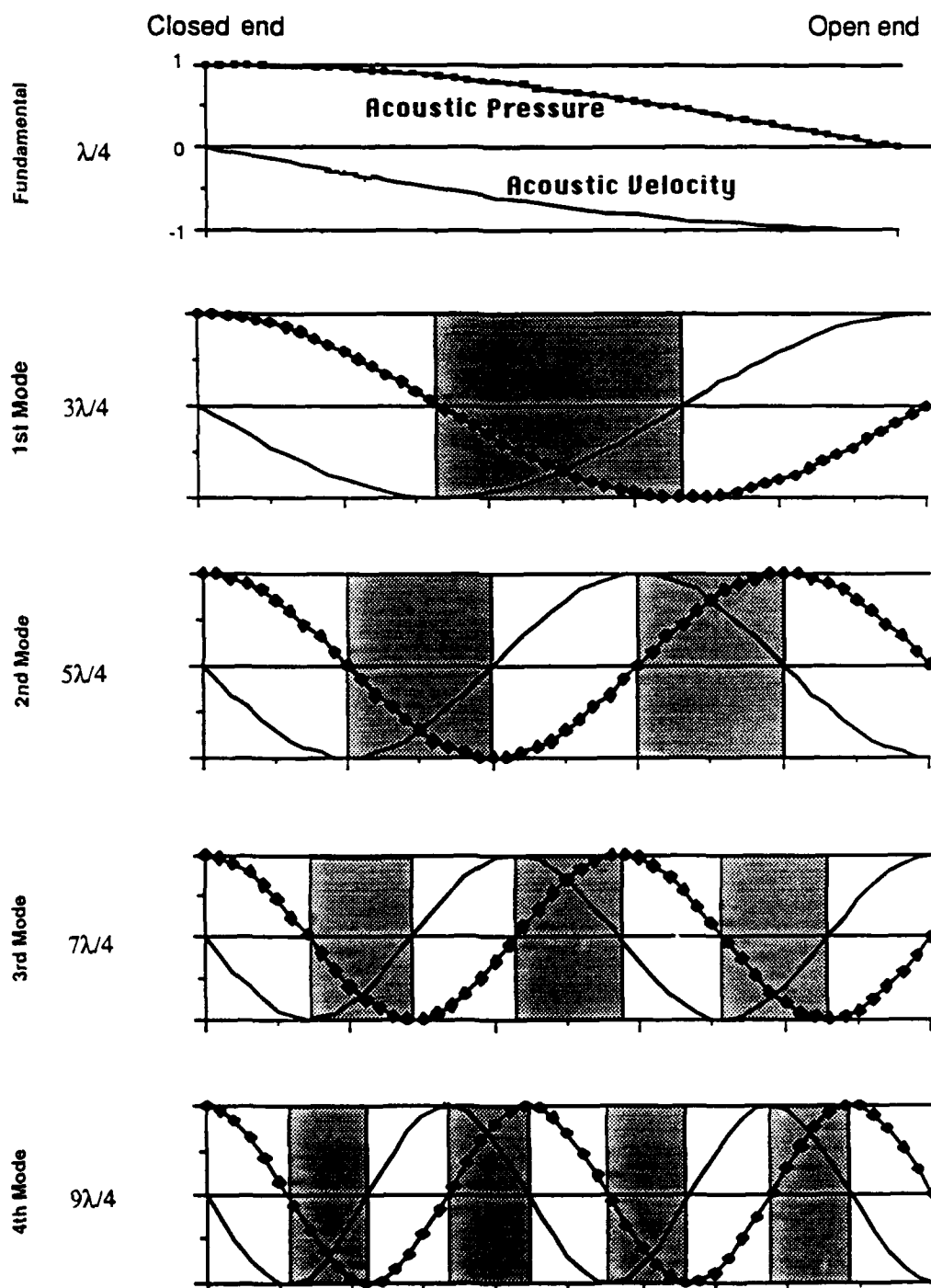
Figure 10. Mode shapes in a closed-open tube which satisfy the criterion for acoustic driving.

3.3 EXPERIMENTAL PROCEDURE

3.3.1 Apparatus

The modified Rijke burner used in these experiments (Figure 11) burns a mixture of propane, oxygen, and nitrogen. Gas flow rates are controlled with precision rotameters. Gases and particles enter the cold section through a small tube, 3 mm i.d., which is located 25 mm from the butterfly valve. The small size of the inlet tube decreases its' acoustical influence and simplifies the boundary condition of the closed end. Although the gas flow is turbulent in the inlet tube, it is believed to be laminar within the burner, where the mean gas velocity is in the range 0.1 to 0.3 m/sec.
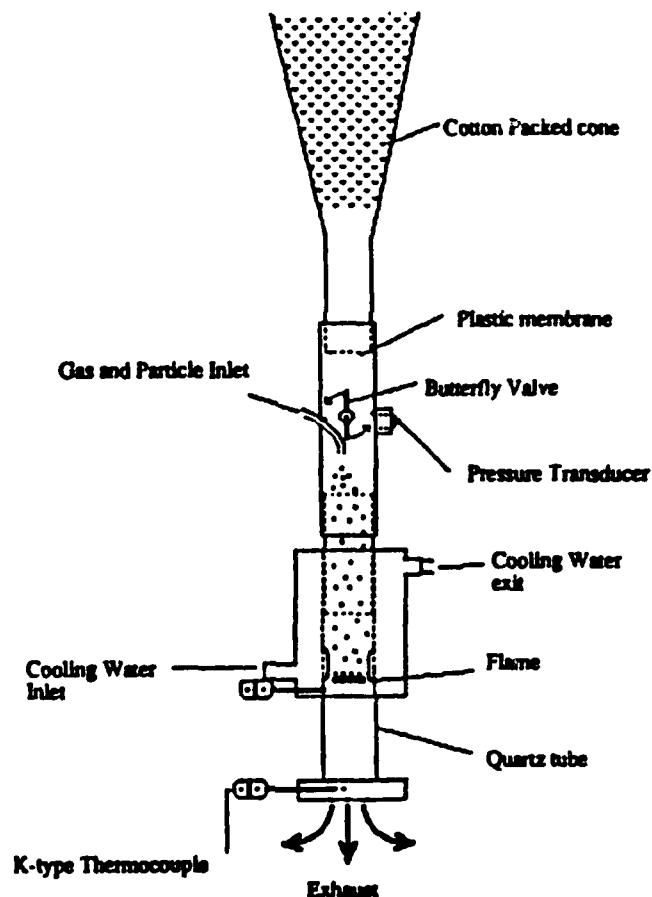
Figure 11. Diagram of the modified Rijke burner apparatus developed at BYU.

The flame is stabilized on a 20 mesh stainless steel screen which is imbedded in thermal conducting putty for enhanced thermal contact with the cooling jacket walls. The flame holder is surrounded by a water-cooled jacket which absorbs heat and helps to prevent flashback. The cold section of the burner has walls of steel or aluminum tubes of 35 mm i.d. The hot section of the burner has walls of optical quality quartz tubes of 37 mm i.d. which allow visual monitoring of the flame. Both the

17

cold section length and the hot section length can be varied by changing tubes. The effective acoustic hot section length can also be varied by changing the product gas temperature, which is controlled by the composition of the inlet gases. The burner may be operated in any orientation, but it was determined that for particle studies, a downward flow within the burner (cold section up and hot section down) would be optimal to assist in particle entrainment.

Major modifications to the previous apparatus include the use of a solenoid-operated butterfly valve at the end of the cold section between the burner and a cotton-packed cone. Cotton packing absorbs the acoustic energy when the valve is open and prevents acoustic growth. Gases are prevented from absorbing in the cotton packing by placing a plastic membrane at the cone entrance. When the valve is closed, oscillations grow. Initially, large fluctuations in the cooling water exit temperature were noted and determined to be caused by air pockets in the cooling jacket. Several modifications have been made to the cooling jacket to ensure a uniform and constant heat transfer. Flow and temperature controllers were installed on the cooling water.

The acoustic pressure oscillations are monitored by high sensitivity pressure transducers (Kistler 606A, PCB 102M75 and PCB 116A11) with impedance converters to reduce the electrical noise. The signal is then amplified and digitized by a Modular Data Acquisition System (MDAS) from TransEra Corp. as shown in Figure 12. The MDAS can sample at rates up to 540 kHz, and can perform spectral analysis using FFT techniques. A relay controls the solenoid, an analog input card reads the voltage amplitude form the pressure transducers, and a thermocouple card reads the voltages from the thermocouples. The pressure transducer is located immediately adjacent to the butterfly valve where there is a pressure antinode. The mode shape has been determined by locating additional transducers along the burner axis.
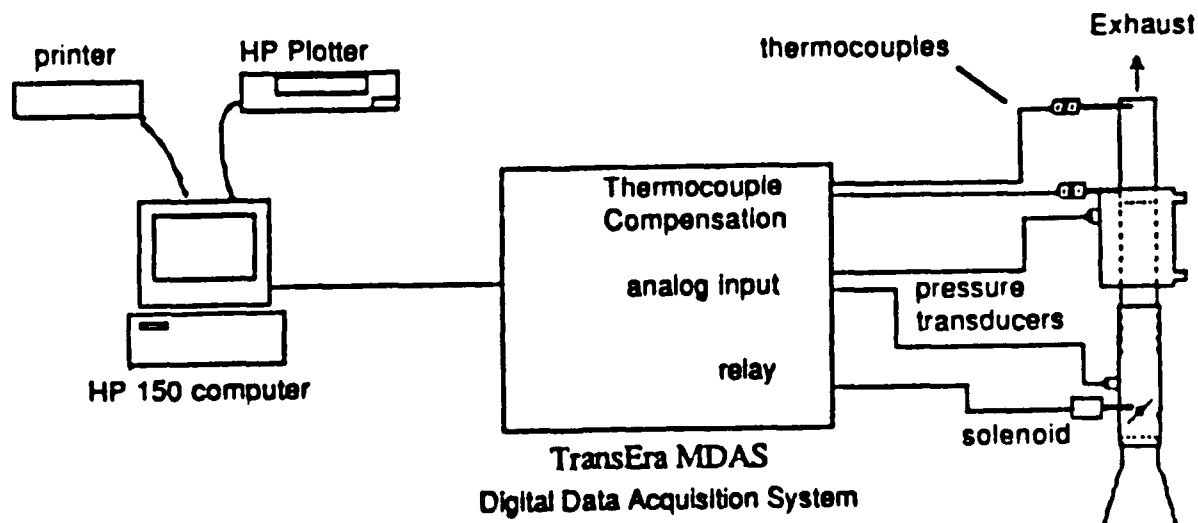
Figure 12. Digital data acquisition system interfaced with the modified Rijke burner and an HP 150 computer.

18

3.3.2 Data Reduction

The digital acquisition system provides a digital sample array containing voltage amplitudes representing the oscillating pressure at discrete time intervals. The more conventional method of plotting the logarithm of pressure versus time is not a practical algorithm for signals represented by digital data. A digital data reduction method was developed to calculate the frequency (ω) and acoustic growth rate (α) for each digital file. This method involves curve fitting the entire acoustic pressure signal, rather than just the pressure peaks. Due in part to mechanical noise in the earliest part of the acoustic oscillation growth period, the pressure signal has an initial amplitude at the start point. The initial acoustic oscillation growth period is a pure sine wave with an exponential growth. These characteristics of the acoustic oscillations can be described by the following equation:[29]

$$P(t) = A e^{\alpha t} \sin(\omega t) \qquad (2)$$

where
P is the entire acoustic signal, as measured by the pressure transducer,

A is the initial amplitude (pressure units),

α is the acoustic growth rate (1/sec),

t is the time (sec), and

ω is the frequency in radians/sec.

A least -squares fit of the digital data to Equation (2) has been used as a suitable method for calculating A and α. Using a nonlinear least-square analysis described by Borse[30], the following equation was developed :

$$\chi^2 = \sum_{i=1}^{N} \frac{(A e^{\alpha t} \sin(\omega (\delta t + t)) - z_i)^2}{(\Delta y_{i,exp})^2} \qquad (3)$$

where
z_i is an array with the data points of interest,

δt adjusts the phase to zero at the starting point,

$\Delta y_{i,exp}$ is the magnitude of the error in the experimental data, and

χ^2 is the sum over all N data points.[30]

Since the magnitude of the error in the experimental data is not currently well defined, $\Delta y_{i,exp}$ was assumed to be constant and eliminated from Equation (3) leaving:

$$\chi^2 = \sum_{i=1}^{N} (A \ e^{\alpha t} \ \sin(\omega \ (\delta t + t)) - z_i)^2 \qquad (4)$$

A multivariable Newton Raphson technique was used to minimize the sum of the squared deviations, (χ^2). The required Jacobian matrix was developed by taking the partial derivative of chi-squared (χ^2) with respect to the two unknown variables A and α. [31]

A typical data set is shown in Figure 13. Note first the noise from the solenoid closing, followed by the growth of the acoustic oscillation from a small amplitude to a limiting amplitude. Only a small portion of the complete data file is of interest in calculating the desired variables A and α. In Figure 13 the region of interest is from data point 365 to 570. The section of the data to be curve fitted is selected by inspection from a screen plot of the complete data file. There are two criteria for selection of the starting point:

1) The starting point is selected as close to the valve closing as possible, and

2) Mechanical noise which may cause "extra" crossings of the x-axis is avoided.

The end point of the data to be fit is selected several cycles before the maximum amplitude is reached.
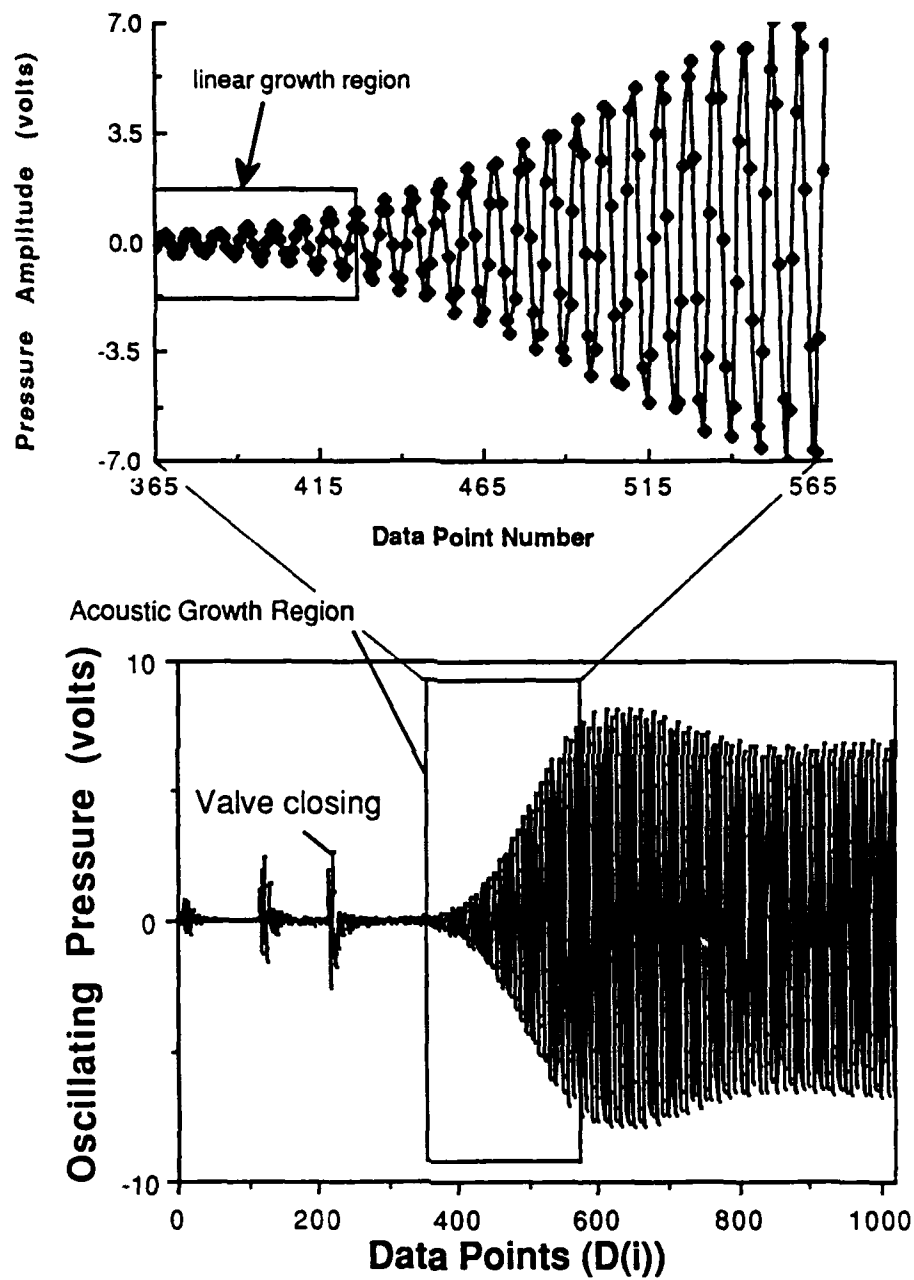
Figure 13. Example data set. Points 365 through 570 are used in z_i curve fitting array.

The computer algorithm calculates a least squares best-fit alpha for the selected set of data points, then drops one cycle of data points and calculates a least squares best-fit alpha for this smaller set of data points. Using the same starting point, the algorithm continues dropping data points from the fit and calculating alphas until only three or four cycles remain. Because the data points on the high end are dropped, the fit gradually approaches the linear growth region as the number of cycles decreases. A plot of the least squares best-fit alpha versus the number of cycles included is shown in Figure 14. The initial linear acoustic growth rate is the desired value, therefore an alpha of 270 is reported for the data in Figure 14. Note that the data becomes more scattered as the number of cycles decreases. This is because the alpha has a high value and because there are fewer cycles in the average. In the linear growth region the fit between the data points and Eq. (1) is usually excellent. A comparison of the resulting least squares best-fit curve with the data points is shown in Figure 15. As the oscillation grows, a limiting amplitude will ultimately be reached, and therefore the recorded α will approach zero for a very large number of cycles.
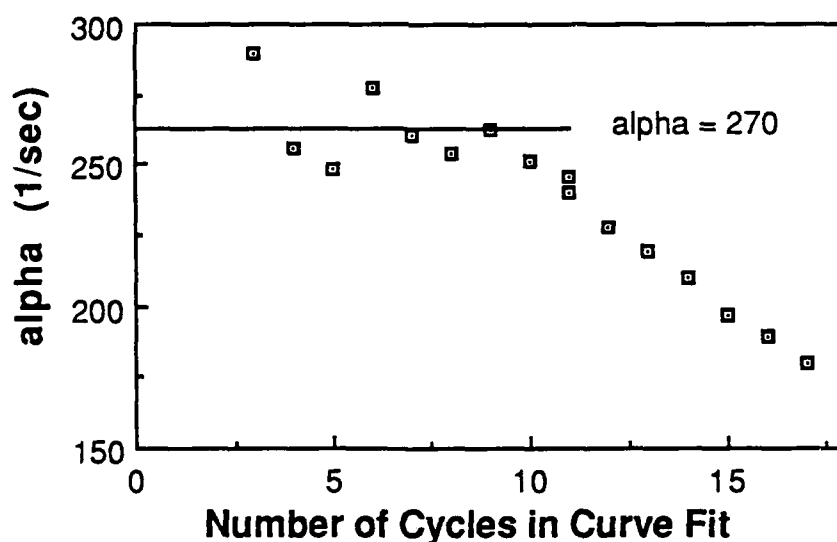
Figure 14. Cycles of the least-square fit vs. alpha. The least squares best-fit alpha "rolls over" after about 10 cycles. The selected acoustic growth rate was 270.

22
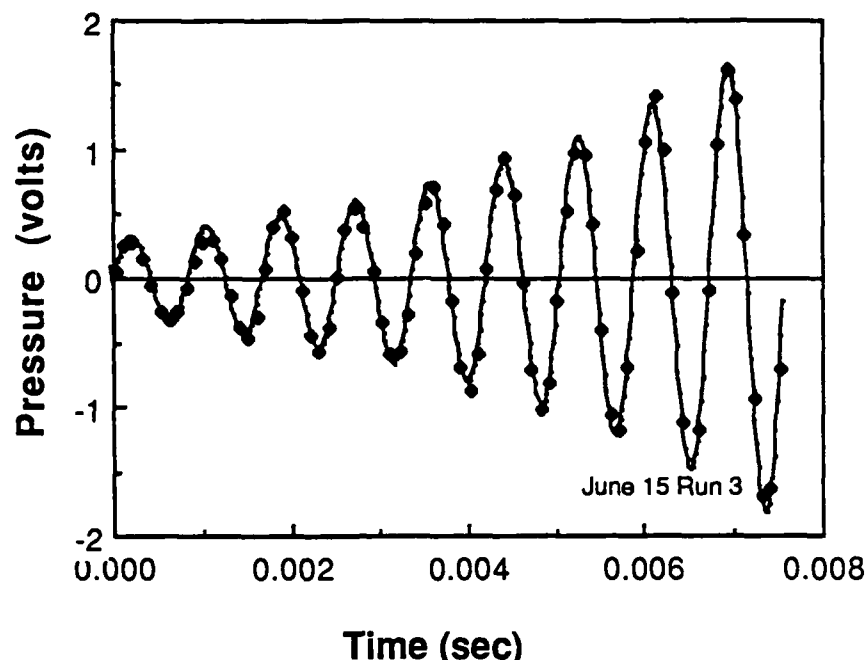
Figure 15. Comparison of mathematical curve fit with the digital data.

3.4 BURNER CHARACTERIZATION

3.4.1 Experimental Observations

During each set of experiments, axial temperature profiles were measured for both oscillating and non-oscillating conditions. The temperatures varied depending on the gas flow rates and the heat transferred from the hot section by radiation and convection. The amplitude of the acoustic oscillations was found to have a strong effect on the convective heat transfer. The data obtained from these experiments have been used to calculate an estimated heat balance for each configuration and define the operational limits of the burner.

Oscillation Limits. In order to compare the burner with previous work by Diederichsen[27], the oscillation limits of the burner were measured for a propane and air mixture with the exhaust down, a hot length of 178 mm, and a cold length of 279 mm. Due to limitations of the gas rotameters, unburnt gas velocities within the burner above 23 cm/sec could not be studied. Figure 16 shows that the lowest air/fuel ratio at which oscillations occurred is 0.73 and the highest air/fuel ratio is 1.27. The unburnt gas velocity must be at least 5 cm/sec within the burner for acoustic oscillations to occur. Diederichsen's[27] results for a similar burner for a methane-air mixture also oriented with the exhaust down showed almost identical results. He found that oscillations could occur at air/fuel ratios between 0.8 and 1.2 and at gas

23

velocities between 8 and 36 cm/sec, depending on the air/fuel ratio and the tube lengths. Because he used a different cold section length, his frequency was slightly lower. However, the results are in good agreement in spite of the minor differences in the closed end boundary conditions, the flame holder configurations, and the fuel.
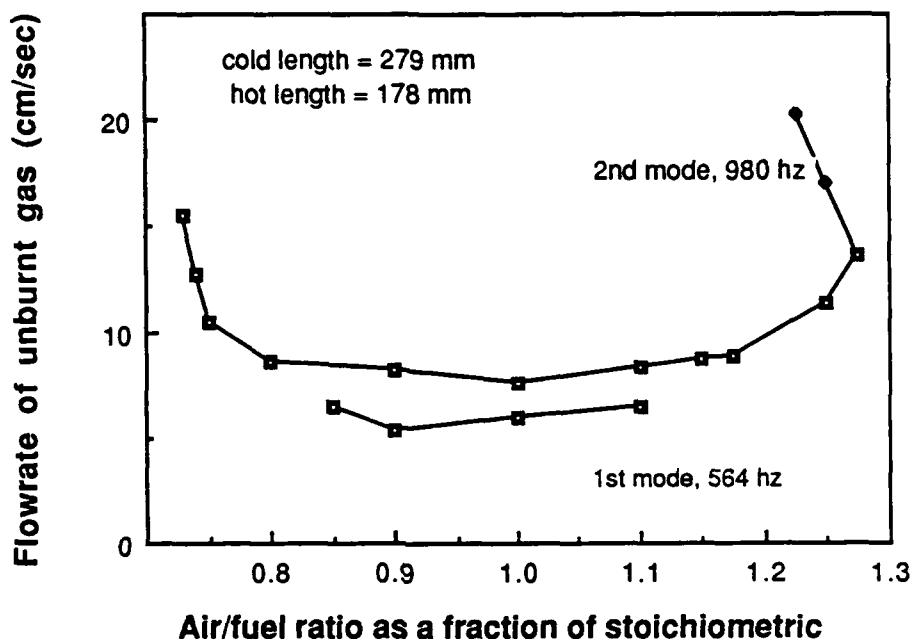
Figure 16. Limits of oscillation for a propane-air mixture in the modified Rijke burner with the exhaust down.

Orientation. The burner was characterized in two different orientations: exhaust up and exhaust down. As was predicted, significant differences in the heat transfer were observed. Figure 17 shows the overall heat balance under identical gas flow and composition conditions for the exhaust up and exhaust down configurations. Note that nearly 500 cal/min additional energy was transferred through the wire gauze into the cooling water for the exhaust down configuration. This additional heat transfer into the cooling water caused an overall downward shift in the temperatures downstream of the wire gauze. The net effect of the temperature shift on the resulting frequency of the oscillating pressure was a shift from the second mode, oscillating at approximately 1200 Hz, to the third mode, oscillating at approximately 1600 Hz. Realizing that the heat transfer was significantly different for the two cases and to allow gravity to assist the particle entrainment, it was decided to operate exclusively in the exhaust down configuration for particle studies.

24
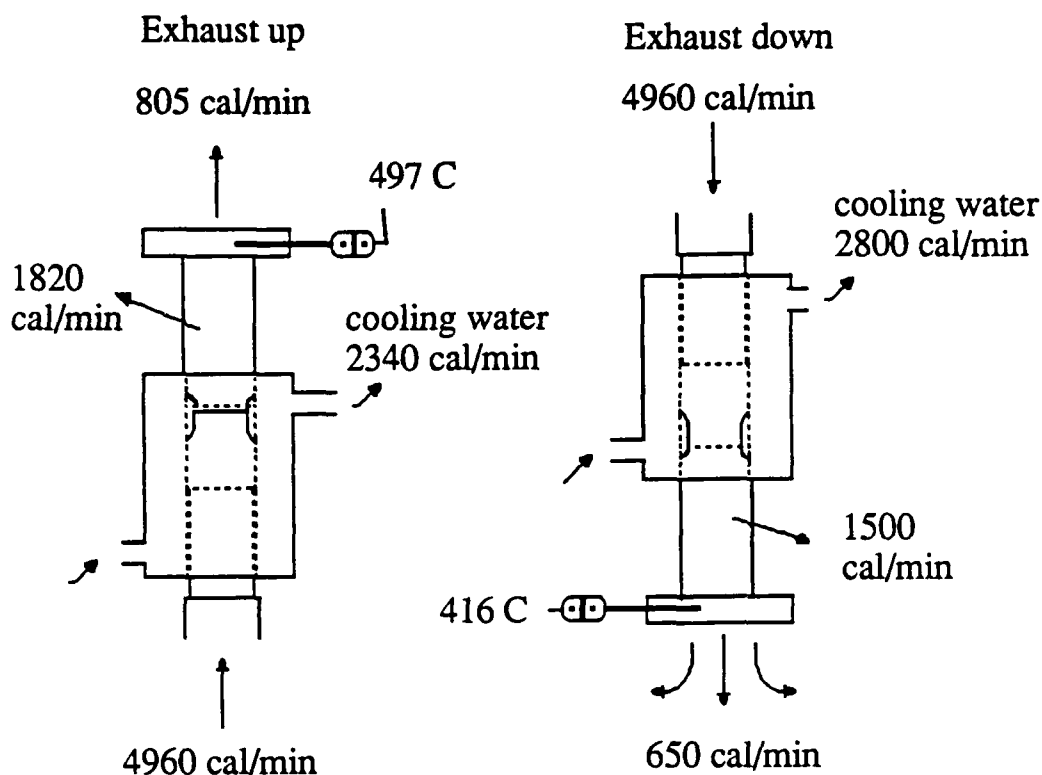
Figure 17. Heat balance of the burner with the exhaust up and exhaust down. (Data from JN15r2, stoich O/F = 1.11, hot length = 106mm, cold length = 266mm, JL30r3, stoich - 1.11, HL = 106, CL = 279 mm)

Increasing the Total Mass Flow Rate. The results of this experimental series are shown in Figure 18. Note that the acoustic growth rate increased within the second mode, until the mode shifted at a total flow rate of approximately 9.5 g/min. The frequency increased about 30 Hz within the second mode due to the increasing temperature profile in the hot section. These observations are due to a combination of the following:

1) The total available energy from the flame increased from 3.9 kcal/min to 7.7 kcal/min. Simultaneously, the exhaust temperature increased from 770K to 1120K, and the heat transferred to the cooling water increased from 1.8 kcal/min to 2.3 kcal/min.

2) The axial temperature profile variation affects the flame position relative to the acoustic driving region.
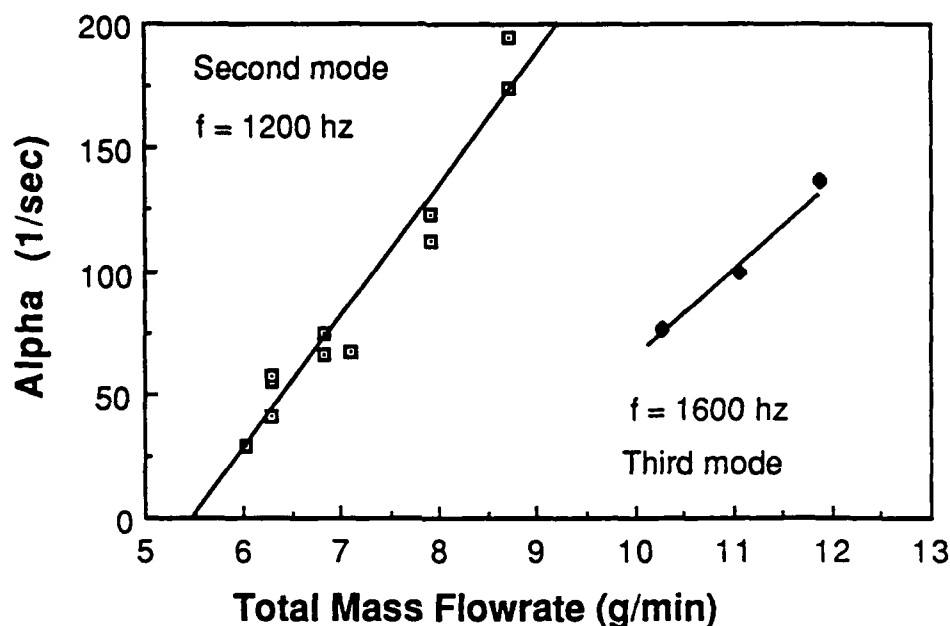
Figure 18   Effect of total mass flowrate at constant gas ratios on alpha.

Increasing O2/F Molar Ratio. In this experiment the propane flow rate was held constant and the oxygen/nitrogen ratio was increased to produce a higher concentration of oxygen. Figure 19 shows the effect of increasing the O_2/F molar ratio. In general, it was noted that additional oxidizer increased the acoustic growth rate up to an O/F ratio of about 1.2. This observation could be explained by a combination of the following:

1)   Thermochemical equilibrium calculations showed the adiabatic flame temperature increasing from 2300K to 2380K as the nitrogen was replaced with oxygen, leading to more total available energy, and perhaps enhanced acoustic coupling with the reaction kinetics.

2)   An increase in the adiabatic flame temperature leads to an increase in the flame speed[32], resulting in a shift of the flame nearer to the wire gauze, hence the heat transferred to the cooling water increased from 2.1 kcal/min to 2.5 kcal/min. The flame holder was observed to glow redder as the O/F ratio increased and the nitrogen decreased. The non-oscillating temperature at the open end dropped from 884K to 763K because of the additional heat transferred to the cooling water.

3)   The axial temperature profile variation shifts the flame position relative to the acoustic driving region. The frequency increased from 1190 to 1200 hz.

Stoichiometric O/F at Constant Total Mass
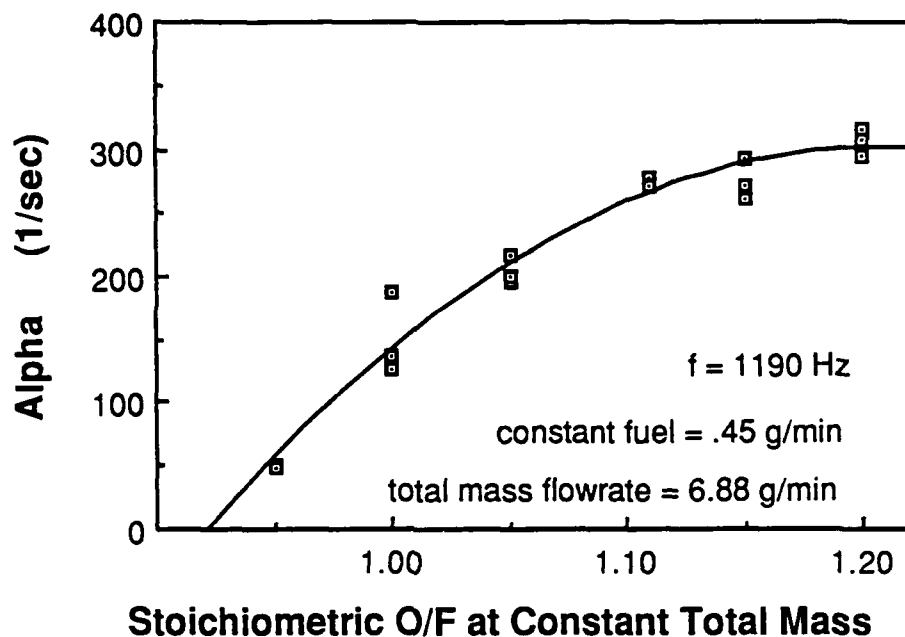
Figure 19.   Effect of O_2/C_3 stoichiometric molar ratio on the acoustic growth rate, alpha.

Increasing the Combustibles to Inerts Ratio.   Holding the total mass flowrate constant at 6.84 g/min and the stoichiometric O_2/C_3 ratio at 1.115, an experimental series was done that varied the ratio of combustible gases to inert gases, $(O_2 + C_3H_8)/N_2$, over a range from 0.40 to 0.58.   This range was defined by the following limitations:

1)   Below a ratio of 0.40, no oscillations were noted, and
2)   Above a ratio of 0.58, the damping system was no longer able to completely dampen the oscillations.

As can be seen in Figure 20, the acoustic growth rate (alpha) increased with increasing $(O_2 + C_3H_8)/N_2$ ratio.   The nonlinear character of the function is probably due to the combination of three dominate effects:

1)   The total available energy of the system increased from 4.5 kcal/min to 5.7 kcal/min with increasing $(O_2 + C_3H_8)/N_2$ ratio,
2)   The heat transfer at the flame holder (wire gauze) into the cooling water increased from 1.8 to 2.7 kcal/min with increasing $(O_2 + C_3H_8)/N_2$ ratio due to the increased flame temperature, and
3)   The axial temperature profile variation shifted the flame position relative to the acoustic driving region, which is demonstrated by a change in the initial growth frequency from 1177 to 1224 hz.   The temperature at the

open end was nearly constant at 783K during the non-oscillating condition, but decreased from 881K to 573K during the oscillating condition as the $(O_2 + C_3H_8)/N_2$ ratio was increased.
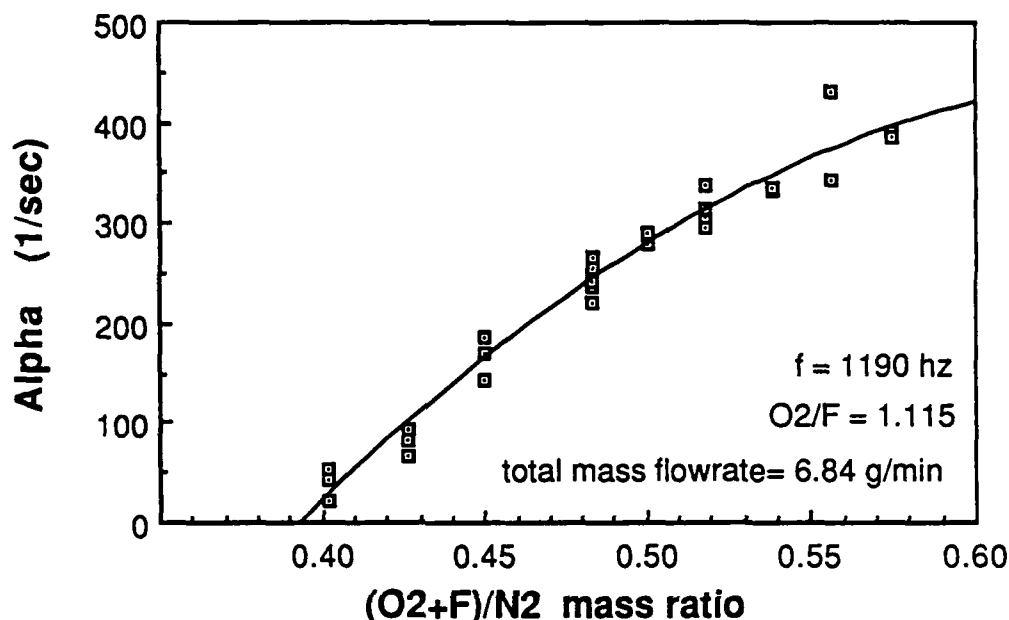
Figure 20. Effect of the combustibles to inerts mass ratio on alpha at a fixed total mass flowrate.

Burner Length. An experiment was performed, varying the cold length of the burner from 245 mm to 437 mm while keeping the hot length constant at 181.5 mm and the gas flow rates constant. As shown in Figure 21 the frequency dropped and then changed from one mode to a higher mode as the total length increased. Figure 21 shows that the acoustic growth rate is a strong function of the cold section length, due to flame position shifts relative to the acoustic pressure and velocity mode shapes as is shown in Figure 10. Three distinctive operating regions are shown in;

1) Cold lengths of 245 mm to 257 mm-the burner oscillated in the first mode,
2) Cold lengths of 257 mm to 270 mm-no oscillations were observed, and
3) Cold lengths of 270 mm to 437 mm-the burner oscillated in the second mode.

The region of greatest interest for future particle studies may be the cold lengths of 320 mm to 360 mm, where the acoustic growth rate is near a maximum over a wide range of lengths. In this region, particle effects can be studied independent of minor heat transfer effects on the mode shape.
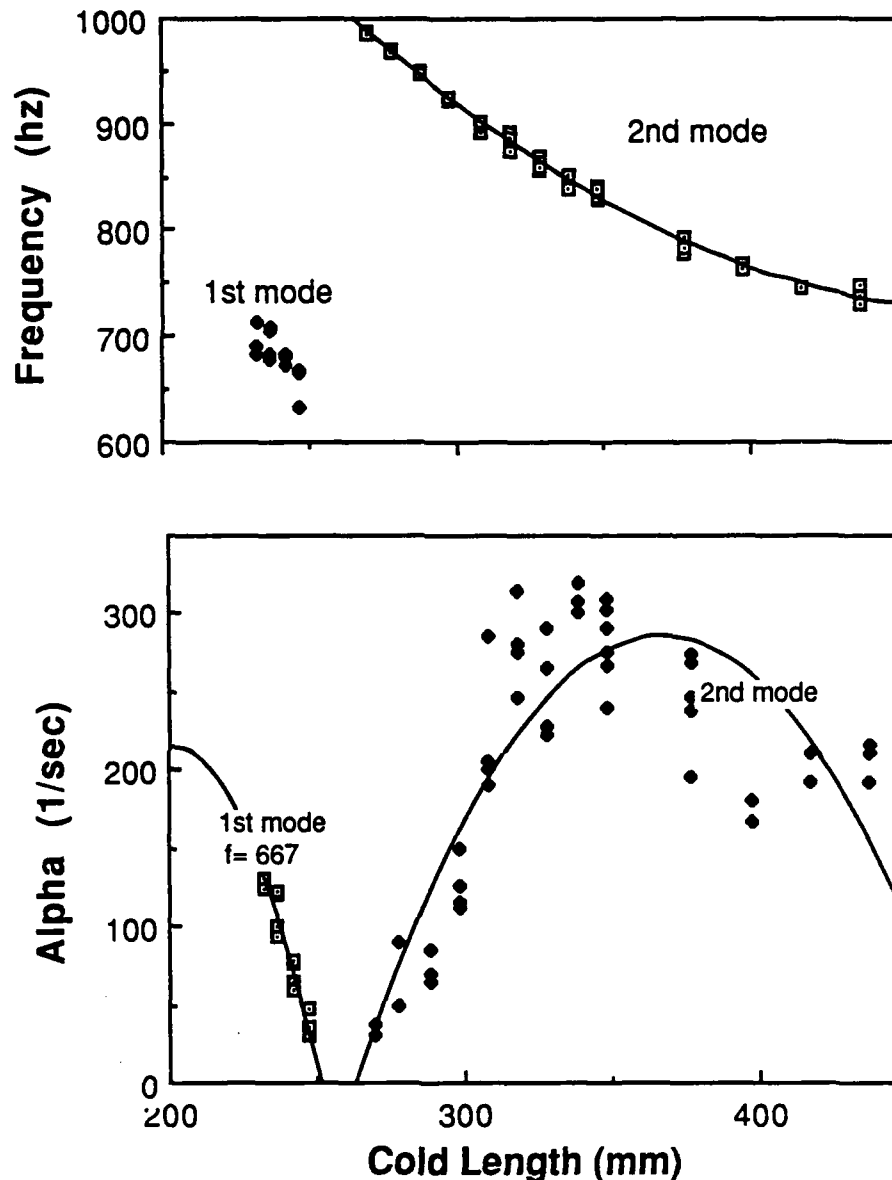
Figure 21. Effect of varying the cold section length on frequency and on alpha at constant gas flowrates. (hot length=182mm, exhaust down)

Radial Profile. The radial temperature profile was measured across the open end of the exhaust using 1/16 " (1.6 mm) K-type thermocouples. The significant heat transfer to the burner walls resulted in a large radial temperature gradient in the hot section as shown in Figure 22. In this configuration, the non-oscillating condition had maximum temperature of 700K, which increased to 880K under oscillating conditions. The radial temperature gradient would naturally result in a radial gas density gradient.
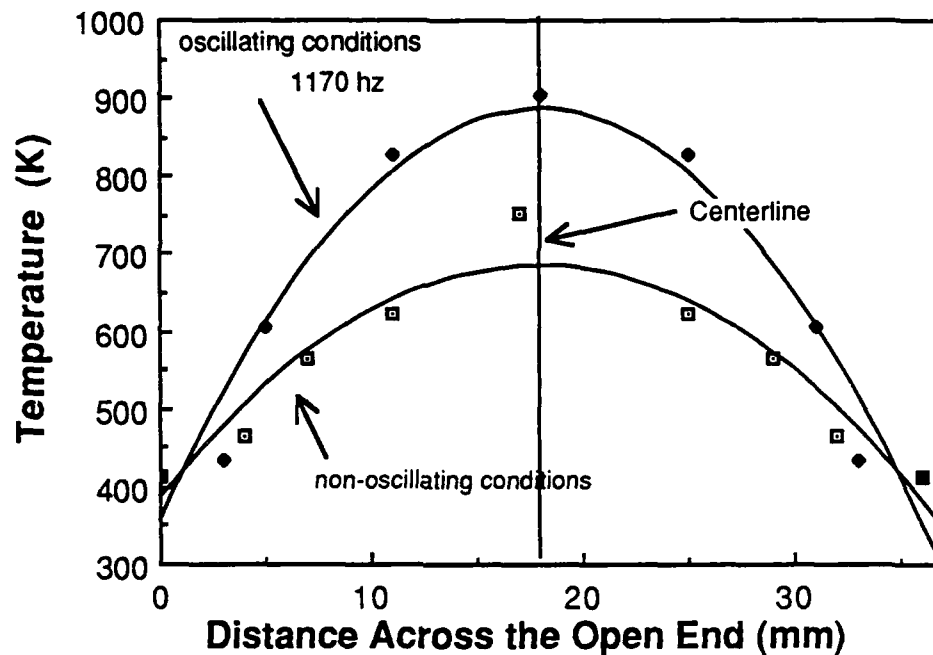
Figure 22. Radial temperature profiles measured at the open end of the burner using 1/16 inch diameter thermocouples.

3.5 EXPERIMENTAL ANALYSIS

3.5.1 Oscillating Heat Transfer Effects

During each experimental run, the oscillations were allowed to continue for 1.5 minutes while recording the temperature profile at regular time intervals. Based on these temperature profiles an approximate oscillating heat balance was calculated. The shift observed in the heat transferred from the hot product gases, reveals that the limiting amplitude of the oscillating acoustic pressure and velocity has a very strong effect on the resulting heat balance. This effect is demonstrated in Figure 23, which was prepared using the data from the variable combustibles to inerts ratio experiments (Figure 20). The change in the heat transferred from the product gases to the cooling water and the burner walls is plotted against the limiting pressure amplitude. For limiting oscillating pressure amplitudes less than 0.06 psi (414 Pa), the heat transferred from the combustion gases to the burner walls decreased, but for limiting amplitudes above 0.06 psi, the heat transferred to the walls increased. The limiting pressure amplitude of 0.06 psi is near the point of gas flow reversal, which occurs when the acoustic velocity amplitude exceeds the mean gas flow.
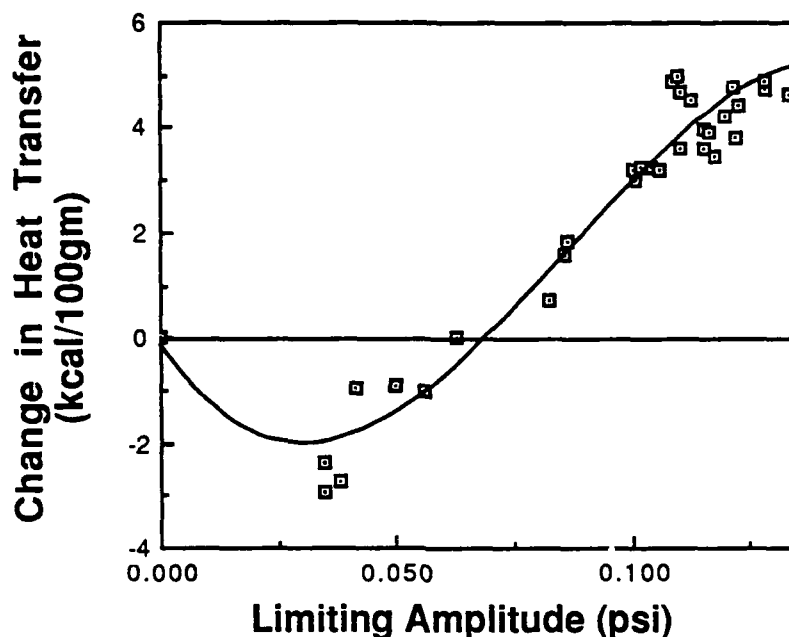
Figure 23. Effect of combustibles to inerts mass ratio on the heat transferred to the burner wall for non-oscillating and oscillating conditions.

A similar phenomena has been observed by Hanby[33] in a study of convective heat transfer in a gas-fired pulsating combustor. Hanby compared the local convective heat transfer coefficients with the values of oscillating pressure amplitude, and hence the velocity amplitude. He found that the convective heat transfer coefficients were approximately constant up to flow reversal and then increased linearly with increasing acoustic velocity amplitude. The combustor he used exhibited organ pipe oscillations very similar to those observed in a Rijke burner.

3.5.2 Overall Heat Balance

Using temperature data from various axial positions along the burner and from the cooling water, an overall heat balance was calculated for each operating condition. Measuring the temperature rise between the cooling water inlet and outlet with a constant flow rate revealed that nearly fifty percent of the combustion energy was transferred to the cooling water. Furthermore, the cooling water flow rate was found to be linearly proportional to the heat transferred over the limited range of water flow rates studied. In this experiment the total combustion energy available was about 4500 cal/min. Increasing the water flow rate from 200 to 900 ml/min caused an additional heat transfer of 700 cal/min into the water, from 1600 cal/min to 2300 cal/min, which represents 16 percent of the total energy or 1 cal /1 ml increase in flow rate. The heat loss through the quartz tube wall along the hot section ranged from 1700 cal/min to 1100 cal/min. Resulting from the heat losses to the cooling water and to the walls of the quartz tube, less than twenty five percent of the heat of combustion

exited the burner exhaust in the combustion products. Naturally, these heat losses affected the temperature profile, the acoustic mode shape, and the resulting frequency of the acoustic oscillations. In fact, it is believed that much of the observed data scatter is the result of uncontrolled heat transfer effects.

3.6 SUMMARY

The acoustic growth rate, alpha (α), of the burner has been characterized experimentally as a function of frequency, flame position, length, inlet gas compositions (O_2, N_2, C_3H_8), and energy balance. The modified Rijke burner allows for measurement of the acoustic growth rate from a non-oscillating to a strongly oscillating environment. The data indicate that the overall acoustic driving forces in a Rijke burner are dependent upon the acoustic mode shape relative to the flame and the distribution of energy, which is a function of the gas flow rates and heat losses. The frequency and acoustic mode shape have been modified by variation of the burner length, flame holder position, cooling water flow rate, inlet gas composition, and inlet gas flow rate. By changing the burner length or reducing the net energy density by the addition of inert gases, the flame shifts from a position of maximum driving and the acoustic growth rate is reduced.

4.0 A NUMERICAL MODEL FOR THE RIJKE BURNER

4.1 INTRODUCTION

The mathematical model for the Rijke burner has been developed to aid in interpretation of experimental data. Varying temperature in the hot (burned gas) section and particle interactions are included in this model. Past models for the Rijke burner and related devices have ignored heat loss in the hot gas section[34-39]. Without heat loss, the temperature in the hot section is constant. The ability to apply the constant temperature assumption is enticing. An analytical solution to the governing equations is possible when this assumption is valid.

Neglect of heat loss makes a small impact on predicted frequency (generally less than 10 percent). Based on frequency alone, constant temperature appears to be a valid assumption. However, it will be shown that this assumption is not valid for the Rijke burner. Application of this assumption can lead to serious error in acoustic growth rate predictions.

4.2 APPROACH

The primary information obtained from the Rijke burner is frequency and growth rate of acoustic oscillations. As a result, prediction of these parameters is the primary objective for the numerical model.

The new Rijke burner model was developed form three-dimensional unsteady equations of conservation written for gas and particle phases[40]. These equations include terms representing mass, momentum and energy exchange between gas and particle phases. Several simplifying assumptions were applied to these equations. The most important assumptions are:

1. Friction at tube walls is negligible,
2. Velocity profiles are flat,
3. Particle volume fraction is negligible,
4. Heat conduction and mass species diffusion are negligible compared to convection,
5. Kinetic energy is negligible,
6. The gas phase behaves as an ideal gas,
7. Particle energy is equal to particle enthalpy,
8. Particles are in dynamic equilibrium with gas flow,
9. Oscillations are small in amplitude.

Table 1 lists the equations resulting from the application of assumptions 1 - 8 in the general equations.

TABLE 1

EQUATIONS DESCRIBING GAS AND PARTICLE PHASES IN THE RIJKE BURNER

Continuity

Gas:
$$\frac{\partial \rho_g}{\partial t} + \frac{\partial}{\partial x}(\rho_g u_g) = \sum_j r_{pj} \qquad [A]$$

Particle:
$$\frac{\partial \rho_{pj}}{\partial t} + \frac{\partial}{\partial x}(\rho_{pj} u_{pj}) = -r_{pj} \qquad [B]$$

Momentum

Gas:
$$\rho_g\left(\frac{\partial u_g}{\partial t} + u_g\frac{\partial u_g}{\partial x}\right) = \frac{-\partial p}{\partial x} - \sum_j f_{pj} - \rho_g g + \sum_j r_{pj}(u_{pj} - u_g) \qquad [C]$$

Particle:
$$\rho_{pj}\left(\frac{\partial u_{pj}}{\partial t} + u_{pj}\frac{\partial u_{pj}}{\partial x}\right) = f_{pj} - \rho_{pj} g \qquad [D]$$

Energy

Gas:
$$\frac{\partial p}{\partial t} + u_g\frac{\partial p}{\partial x} = c^2\left(\frac{\partial \rho_g}{\partial t} + u_g\frac{\partial \rho_g}{\partial x}\right) + (\gamma-1)\left[-\sum_j q_{cpj} + \sum_j r_{pj}h_{sj} - \sum_i r_{gi}h_{gi} - \sum f_{pj}(u_{pj} - u_g) + q_{sg}\right] \qquad [E]$$

Particle:
$$\rho_{pj}\left(\frac{\partial h_{pj}}{\partial t} + u_{pj}\frac{\partial h_{pj}}{\partial x}\right) = q_{cpj} - r_{pj}(h_{sj} - h_{pj}) + q_{spj} \qquad [F]$$

Equations for oscillating properties (i.e. pressure, gas and particle velocity and temperature) were developed from the Table 1 equations. The first step was to represent each property as the sum of two components: a time-independent mean component, $\bar{\phi}$, and an oscillating component, ϕ'. The equations were expanded to give terms of various orders in oscillating properties. All zero-order terms (i.e. terms containing only mean properties) were eliminated by subtracting the mean property conservation equations. Terms higher than first order in oscillating quantities were neglected in accordance with assumption 9.

The result of these operations is a set of partial differential equations describing oscillating properties. Solutions to these equations were assumed to be of complex exponential form:

$$\phi'(x,t) = \hat{\phi}(x)e^{i\omega t} \qquad (4)$$

where ω is a complex number. Solutions of this form were inserted into the partial differential equations. This reduced the equations to the set of ordinary differential equations listed in Table 2. These equations apply to gases and particles in both cold and hot sections of the tube.

TABLE 2

EQUATIONS FOR OSCILLATING GAS AND PARTICLE PROPERTIES
WITH SINUSOIDAL TIME-DEPENDENCY REMOVED

Continuity

Gas:

$$\frac{d\hat{u}_g}{dx} = \frac{-1}{\bar{\rho}_g} [(\frac{d\bar{u}_g}{dx} + i\omega)\hat{\rho}_g + \frac{d\bar{\rho}_g}{dx}\hat{u}_g - \sum_j \hat{r}_{pj}] \tag{A}$$

Particle:

$$0 = (\frac{du_{pj}}{dx} + i\omega)\hat{\rho}_{pj} + \frac{d\bar{\rho}_{pj}}{dx}\hat{u}_{pj} + \hat{r}_{pj} \tag{B}$$

Momentum

Gas:

$$\frac{d\hat{p}}{dx} = -(\bar{u}_g\frac{d\bar{u}_g}{dx} + g)\hat{\rho}_g - \bar{\rho}_g(\frac{d\bar{u}_g}{dx} + i\omega)\hat{u}_g - \sum_j \hat{f}_{pj} + \sum_j \bar{r}_{pj}(\hat{u}_{pj} - \hat{u}_g) + \sum_j \hat{r}_{pj}(\bar{u}_{pj} - \bar{u}_g) \tag{C}$$

Particle:

$$0 = (\bar{u}_{pj}\frac{d\bar{u}_{pj}}{dx} + g)\hat{\rho}_{pj} + \bar{\rho}_{pj}(\frac{d\bar{u}_{pj}}{dx} + i\omega)\hat{u}_{pj} - \hat{f}_{pj} \tag{D}$$

Energy

Gas:

$$0 = c^2(\frac{d\bar{u}_g}{dx} + i\omega)\hat{\rho}_g - (\gamma\frac{d\bar{u}_g}{dx} + i\omega)\hat{p} + c^2\frac{d\bar{\rho}_g}{dx}\hat{u}_g + (\gamma-1)[\sum_j \hat{q}_{cpj} + \sum_j \bar{r}_{pj}\hat{h}_{sj}$$

$$+ \sum_j \hat{r}_{pj}\bar{h}_{sj} - \bar{T}_g(\sum_i \bar{r}_{gi}c_{pgi} - c_{pg}\sum_j \hat{r}_{pj}) + \hat{q}_{sg}] \tag{E}$$

Particle:

$$(\bar{r}_{pj} - i\omega\bar{\rho}_{pj})\hat{h}_{pj} - (\bar{u}_{pj}\hat{\rho}_{pj} + \bar{\rho}_{pj}\hat{u}_{pj})\frac{d\bar{h}_{pj}}{dx} + \hat{q}_{cpj} + \hat{q}_{spj} - \bar{r}_{pj}\hat{h}_{sj} - \hat{r}_{pj}(\bar{h}_{sj} - \bar{h}_{pj}) = 0 \tag{F}$$

The solution to the differential equations of Table 2 is obtained by integration and application of boundary conditions. A nontrivial solution can only be obtained for certain values of the parameter ω. These values are members of a set of complex eigenvalues. The real part of one of these eigenvalues give the frequency of a possible Rijke mode. The imaginary part is the negative of the growth rate for that mode.

35

Boundary conditions are required at the tube ends and at the flame interface. The acoustic boundary at the open end is actually two-dimensional in nature. However, the boundary condition can be approximated one-dimensionally. The tube is treated as if it were 0.613R (R being the tube radius) longer than in fact, and $\hat{P}$ (the oscillating component of the pressure) is set to zero. At a closed end, $\hat{u}$ is set equal to zero.

Assuming that the flame thickness is small, the flame can be treated as a discontinuity. Equations for continuity of oscillating properties across the interface are listed in Table 3. These equations were developed from general interface conservation equations[41].

For simple Rijke burner configurations (e.g. constant temperature in each tube section), the equations of Table 2 can be integrated analytically. Application of boundary and interface conditions gives a set of simultaneous algebraic equations. Eigenvalues can be calculated from this set of equations by any suitable iterative technique.

In general, the acoustic equations can not be integrated analytically for complex Rijke burner configurations. As a result, numerical methods must be used to obtain eigenvalues from the differential equations of Table 2. A FORTRAN77 program (RIJKE.FOR) has been written for this purpose.

The algorithm used to calculate eigenvalues is based on the "shooting method" for integrating boundary value problems[42]. The procedure is illustrated in the flowchart of Figure 24. The first step in the process is to calculate mean properties (i.e. mean gas and particle density and velocity, etc.) throughout the Rijke tube. The frequency of the fundamental mode is estimated form the mean temperature profile.

The next step is estimation of an eigenvalue. In a tube filled with a uniform temperature gas, the frequency of each mode is a multiple of the fundamental mode. In a tube filled with a varying-temperature gas, frequencies of higher modes may not be exact multiples of the fundamental frequency. However, a reasonable assumption is that higher-mode frequencies will be close to multiples of the fundamental. Therefore a multiple of the fundamental frequency is used as initial estimate of the real part of the eigenvalue. The imaginary part of the eigenvalue is set to zero.

Using the estimated eigenvalue, the acoustic equations of Table 2 are numerically integrated. Integration begins with the acoustic boundary conditions at the bottom of the tube. The integration steps upward through the tube until the flame interface is reached. At this point, the acoustic interface conditions of Table 3 are used to traverse the flame. The stepwise integration is resumed and is terminated when the tube exit is reached.
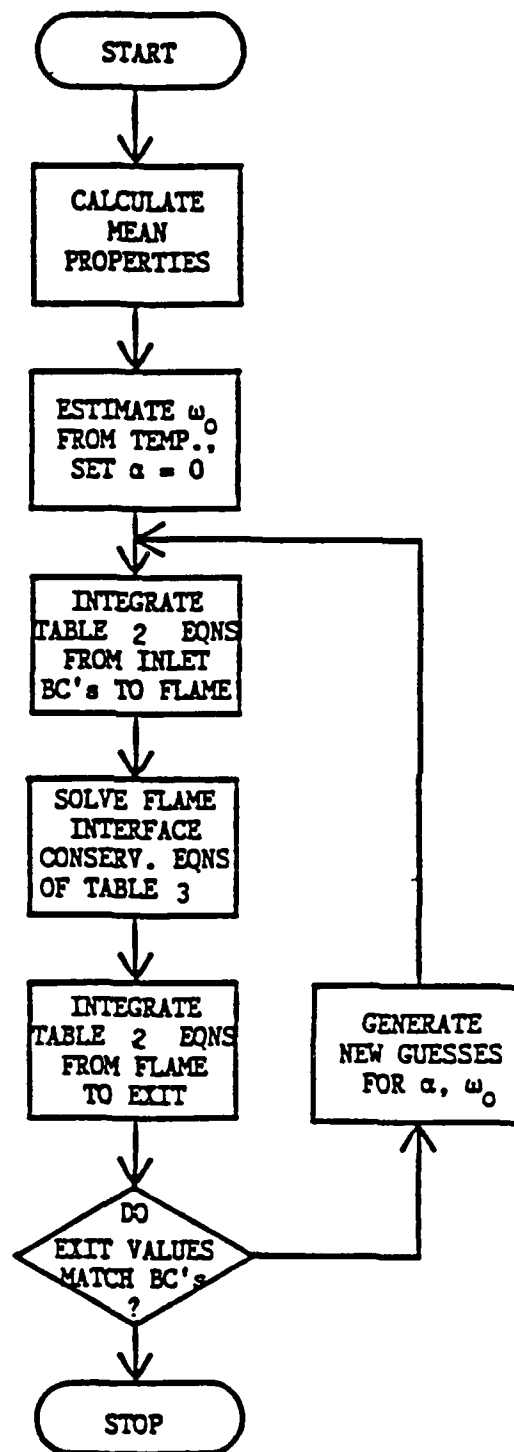
Figure 24. Flowchart of algorithm used in program to calculate rijke burner eigenvalues.

TABLE 3

OSCILLATING INTERFACE CONSERVATIONS CONDITIONS FOR GAS AND PARTICLE
PHASES WITH TIME DEPENDENCY REMOVED

Continuity

Gas:
$$\bar{\rho}_{g2}\hat{u}_{g2} = \bar{\rho}_{g1}\hat{u}_{g1} + (\bar{\rho}_{g2} - \bar{\rho}_{g1})\hat{u}_i \qquad [A]$$

Particle:
$$\bar{u}_{pj2}\hat{\rho}_{pj2} + \bar{\rho}_{pj2}\hat{u}_{pj2} = \bar{u}_{pj1}\hat{\rho}_{pj1} + \bar{\rho}_{pj1}\hat{u}_{pj1} + (\bar{\rho}_{pj2} - \bar{\rho}_{pj1})\hat{u}_i \qquad [B]$$

Momentum

Gas:
$$\hat{P}_2 = \hat{P}_1 \qquad [C]$$

Particle:
$$\bar{\rho}_{pj2}\bar{u}_{pj2}\hat{u}_{pj2} = \bar{u}_{pj1}(\bar{u}_{pj2} - \bar{u}_{pj2})\hat{\rho}_{pj1} + \bar{\rho}_{pj1}(2\bar{u}_{pj1} - \bar{u}_{pj2})\hat{u}_{pj1} + \bar{u}_{pj2}(\bar{\rho}_{pj1} - \bar{\rho}_{pj2})\hat{u}_i \qquad [D]$$

Energy

Gas:
$$\bar{\rho}_{g2}\bar{u}_{g2}C_{pg2}\hat{T}_{g2} = \rho_{g1}\bar{u}_{g1}C_{pg1}\hat{T}_{g1} + \bar{\rho}_{g1}(\bar{h}_{g2} - \bar{h}_{g1})(\hat{u}_i - \hat{u}_{g1}) \qquad [E]$$

Particle:
$$\bar{\rho}_{pj2}\bar{u}_{pj2}\hat{h}_{pj2} = \bar{\rho}_{pj1}\bar{u}_{pj1}\hat{h}_{pj1} + \bar{u}_{pj1}(\bar{h}_{pj1} - \bar{h}_{pj2})\hat{\rho}_{pj1} + \bar{\rho}_{pj1}(\bar{h}_{pj2} - \bar{h}_{pj1})(\hat{u}_i - \hat{u}_{pj1}) \qquad [F]$$

Exit boundary conditions are compared to exit values resulting from the integration process. A perfect match indicates that the estimated eigenvalue was correct. Incorrect eigenvalues are refined by a complex-valued Newton's method. The refinement process is repeated until the change in the eigenvalue is less than a specified error tolerance.

4.3 MODEL CALIBRATION

To evaluate the validity of the model, the Rijke burner computer program has been run for a number of simple test cases[22]. The cases consist of situations for which analytical solutions to the equations of Table 2 are possible. Cases for particle

damping are obtained from literature sources[43,44]. Rijke tube configurations for which analytical solutions were obtained include:

1. A tube with uniform temperature throughout,
2. A tube with uniform but different temperatures in the hot and cold sections,
3. A tube with a heat release region of finite thickness located between constant-temperature hot and cold sections,
4. A tube with a parabolic temperature profile.

None of these test configurations included acoustic interactions due to the flame. Frequencies predicted by the program matched test case values to within 0.1%, and growth rates matched to within 2%[22]. This establishes the accuracy and validity of the solution algorithm.

4.3.1 Comparison of Flame Response Models

The program has been used to investigate the effect of heat loss on acoustic oscillations. Growth rate predictions for configurations with and without heat loss were compared. The temperature profiles for the two cases are illustrated in Figure 25. The temperature profile for the heat loss case is an exponential curve fit through the experimental data. The heat transfer coefficient used in the program was obtained from the curve fit.
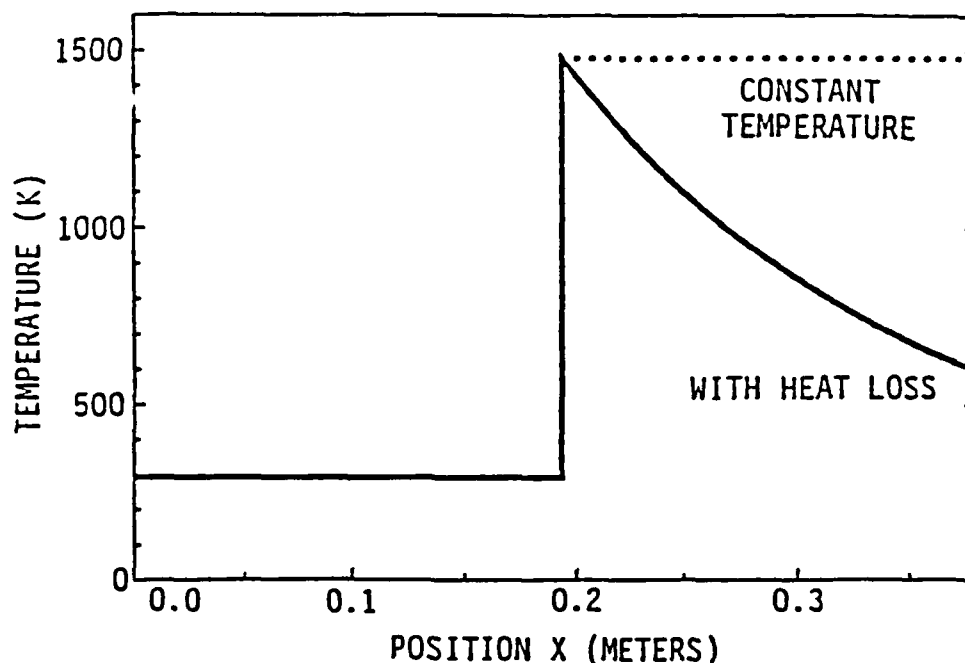
Figure 25. Temperature profiles used for comparison of flame response models.

The tube geometry matched one configuration used previously by Braithewaite and Beckstead[20]. The total tube length and diameter were 36.5cm and 3.81cm, respectively. Properties in the cold section were for a mixture of 5.3% propane, 27.2% oxygen and 67.5% nitrogen. All hot section properties except flame temperature were for the gas mixture resulting from adiabatic combustion of the cold section gases. Flame temperature was obtained from the exponential curve fit.

Flame models of Merk[45-47] and Bailey[36] were used to model the fluctuating flame velocity, u, in the acoustic interface equations of Table 3. From Merk's equations, u is given by:

$$\hat{u}_i = (\frac{\Lambda}{1 - \Lambda}) \, (\frac{1 - B}{B}) \, (\frac{1 + i/(\omega_o \tau)}{1 + 1/(\omega_o \tau)^2}) \, \hat{u}_1 \qquad (5)$$

where $\Lambda = \overline{p}_1/\overline{p}_2$, $B = C_{p2} \overline{T}_2/C_{p1}\overline{T}_1$, ω_o is the real frequency of oscillation and τ is a time lag characteristic of the flame. From Bailey's equations, u_i is given by:

$$\hat{u}_i = (\frac{1 + i\delta}{1 + \delta^2}) \, \hat{u}_1 \qquad (6)$$

where $\delta = \sigma/\omega_o$ and σ is the derivative of the flame speed with respect to distance between the flame and gauze. If the ratio of specific heats in the two sections is the same A = B and Equation (5) reduces to Equation (6) with $\sigma = 1/\tau$. As a result, the models of Bailey and Merk are essentially equivalent.

For the experimental configuration duplicated in the program runs, Braithewaite and Beckstead measured frequencies around 735 Hz for the second mode of oscillation. Growth rates for gas without particles were around 335 sec^{-1}.

Using Equation (6), the program was run for the second mode of oscillation. Several values of σ were used. The results for cases with and without heat loss are illustrated in Figure 26. Figure 26 shows that when heat loss is taken in to account, Bailey's flame response model can produce frequencies and growth rates comparable to those obtained experimentally for some values of σ. When heat loss is ignored, the model predicts negative growth rates for all values of σ. As a result, accounting for heat loss is critical to accurate prediction of growth rates.
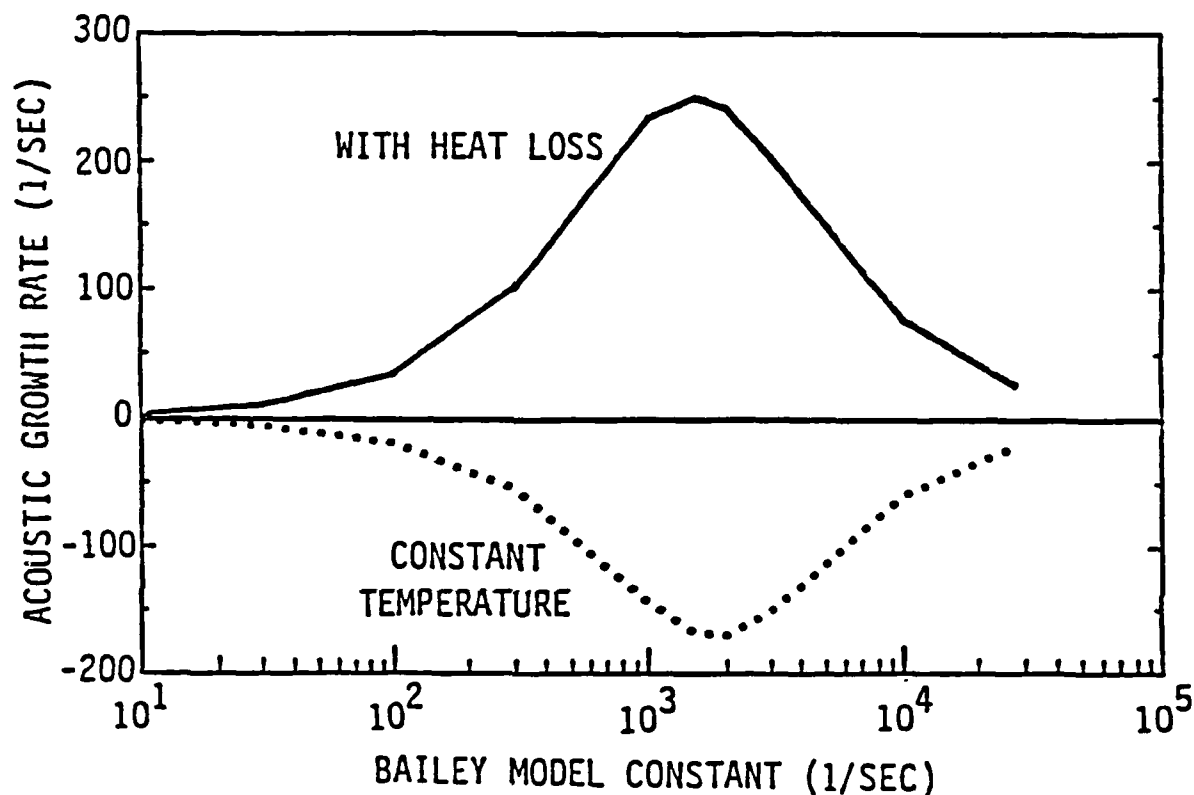
Figure 26. Plot of growth rate versus Bailey model constant.

The reason why heat loss drastically effects growth rate predictions is illustrated in Figure 27. Figure 27 shows calculated acoustic pressure and velocity profiles for the second mode of oscillation with and without heat loss. Heat loss causes distortion in the shape of these profiles due to its effect on the speed of sound. Speed of sound is proportional to the one-half power of temperature. Therefore, as temperature drops, so does the speed of sound. This causes the nodes and antinodes to move toward the exit of the tube relative to the constant temperature situation.
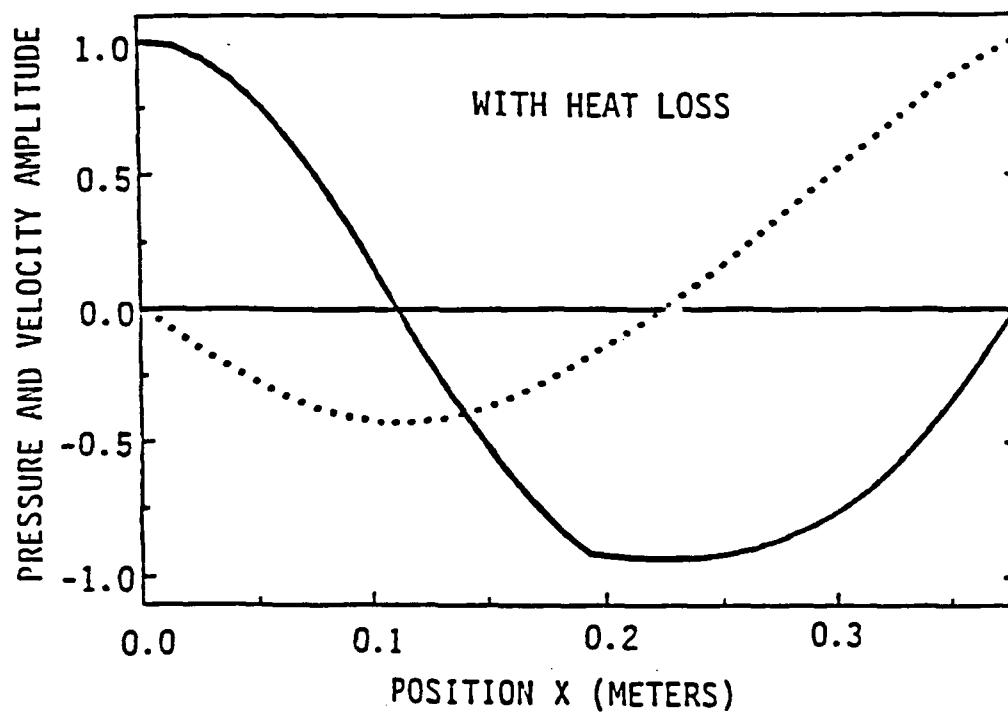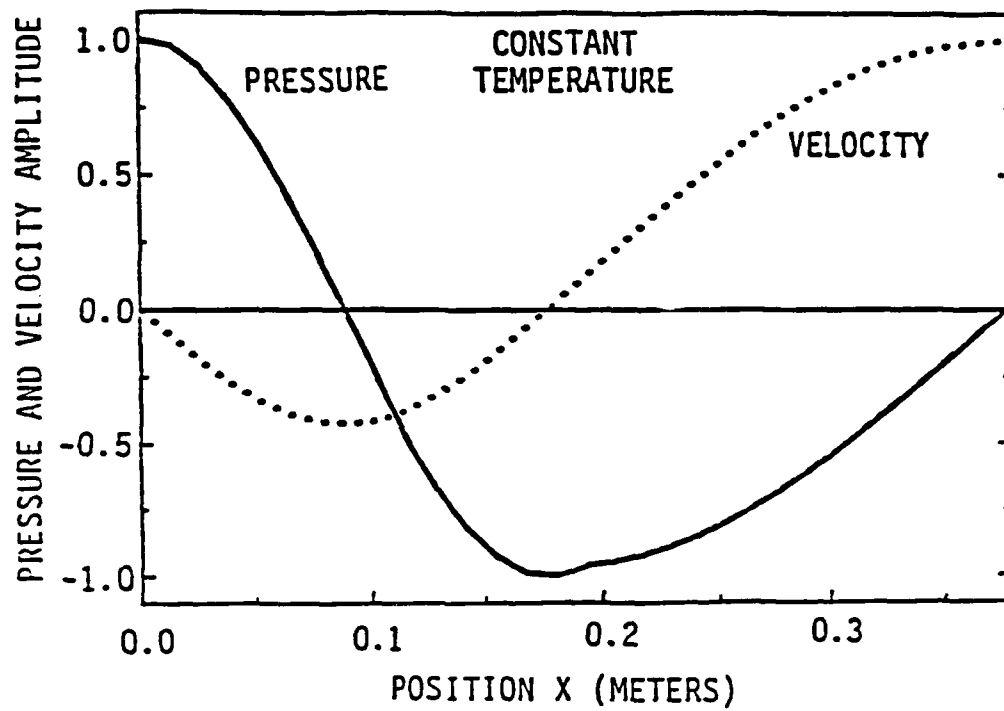
Figure 27. Acoustic pressure and velocity amplitude for constant temperature and heat loss cases.

The form of Equations (5) and (6) indicate that acoustic growth rate is governed by the value of *acoustic velocity at the flame*. *From Figure 27 it can be seen that* acoustic velocity at the flame is of opposite sign for the cases with and without heat loss. This sign reversal is responsible for the change in sign of the acoustic growth rate.

In his model, Bailey assumed that flame speed adjusts instantly when the flame is moved to a new distance from the gauze. A simple modification of Equation (6) is obtained by relaxing the assumption of instantaneous flame response:

$$\hat{u}_i = (\frac{1 - \delta\omega_o\tau + (\omega_o\tau)^2 + i\delta}{1 + (\delta - \omega_o\tau)^2}) \, \hat{u}_1 \qquad (7)$$

where τ is a time lag associated with the adjustment of flame speed. Equation (7) reduces to Equation (6) when $\tau = 0$.

By adjusting the parameters σ and τ in Equation (7), the program can predict the experimentally observed frequency and growth rate of 735 Hz and 335 sec^{-1} exactly. *The values of σ and τ for which this occurs are 996.8 sec^{-1} and 1.983x10^{-4}* sec, respectively. Using the same values of σ and τ, the program predicts a frequency and growth rate of 168 Hz and -332 sec^{-1} for the first mode of oscillation and 1353 Hz and 60 sec^{-1} for the third. These results agree qualitatively with experimental observations. The second mode with the highest growth rate is observed. The first mode with a negative growth rate is strongly damped and does not appear. The third mode has a relatively small positive growth rate. The third mode will grow more slowly than the second and due to nonlinear effects may never be observed.

The modified Bailey model shows promise for modeling flame response in the Rijke burner. Further comparison with experiment to fully understand the physical significance of the parameters σ and τ will be presented in a later section.

4.4 RESULTS OF PARTICLE COMBUSTION

Preliminary results have been obtained fro the effects of aluminum particle combustion in the Rijke burner. A modification of the diffusion flame model found in Glassman[32] was used to describe aluminum combustion. This model assumes that diffusion around the particle is very rapid.

Table 4 shows a comparison of results from the program to experimental data. The values in Table 4 are additional growth rate due to particle combustion. These values were obtained by subtracting growth rate due to gas alone from the growth rate due to particle and gas. As can be seen, the additional driving predicted by the

program is of the correct sign and trend but is an order of magnitude too small. This discrepancy may be due to the rapid diffusion assumption. Factors responsible for the discrepancy will be investigated in future work.

TABLE 4

COMPARISON OF EIGENVALUES PREDICTED BY RIJKE TO DATA OF
BRAITHEWAITE AND BECKSTEAD FOR 1, 2 AND 5% 13µ Al

| | Exper. Data | | Predictions | |
C_m	ω_0 (Hz)	$\Delta\alpha$ (1/sec)	ω_0 (Hz)	$\Delta\alpha$ (1/sec)
0.0094697	~4618	82.	4653	1.233
0.020	▪	137.	4603	7.214
0.050	▪	251.	4478	33.87

4.5 CONCLUSIONS

A mathematical model for the Rijke burner has been developed. This model accounts for the effects of heat loss and particle interactions on acoustic oscillations. The model correctly predicts frequency and growth rates for several simple test cases.

In this work, acoustic response of the Rijke burner flame has been approximated using a simple model developed by Bailey. A model developed by Merk has been shown to be essentially equivalent to Bailey's model. These models do a fair job of predicting acoustic growth rate when heat loss is taken in to account. The ability of these models to predict reasonable growth rates is critically dependent on use of an accurate acoustic mode shape.

To accurately estimate the acoustic mode shape, temperature variation must be taken into account. Models which assume constant temperature will not predict the correct mode shape. As a result, assuming constant temperature could lead to the erroneous conclusion that Bailey's model does not work.

An extension of the Merk and Bailey model has been developed. Experimentally-measured frequency and growth rate can be matched exactly by adjusting the two parameters in this model.

44

5.0 DATA ANALYSIS USING RIJKE COMPUTER MODEL

The RIJKE.FOR computer model was used to interpret experimental data. The dimensions, flow rates, and temperatures of the burner were input, then the flame parameters τ and σ were adjusted to fit the variable cold length data set. The model was expected to predict the correct trends, but not the exact values, because it is a 1st order perturbation model and doesn't attempt to model all the physical phenomena. The resulting plots provide insight into the acoustic oscillations that is difficult to achieve by other methods of analysis. The variable cool section length data set was selected for modeling for two reasons:

1.   The gas flow rates were held constant in each test, therefore
     a.   Data preparation was simplified, and
     b.   The flame parameters were constant for the entire data set.
2.   The oscillations changed from the first mode to the second mode, giving the model a thorough test.

5.1 Mean Gas Property Prediction

A unique strength of Raun's RIJKE model is its ability to match the measured temperature decrease in the hot section as the gases cool through heat transfer to the walls. The temperature profile is approximated in the computer model by adjusting values of the inlet enthalpy and overall heat transfer coefficient. Matching the temperature profile and using a small end correction, the measured frequency can be consistently matched within $\pm$ 3 percent. The cool section was modeled with a constant temperature of 297K, assuming an instantaneous temperature rise at the flame holder. Figure 28 shows the predicted mean temperature, velocity, and Reynolds number profiles along the burner with a cool section length of 225 mm and a hot section length of 181 mm. At the flame, the mean temperature increased from 297K to 1200K, the velocity increased from 11 to 45 cm/sec, and the Reynolds number decreased from 350 to 100. Clearly, the Reynolds number is in the laminar region. Simultaneously, the Prandtl number increased from 0.74 to 0.78 and the speed of sound increased from 350 to 660 (m/sec) across the flame holder.
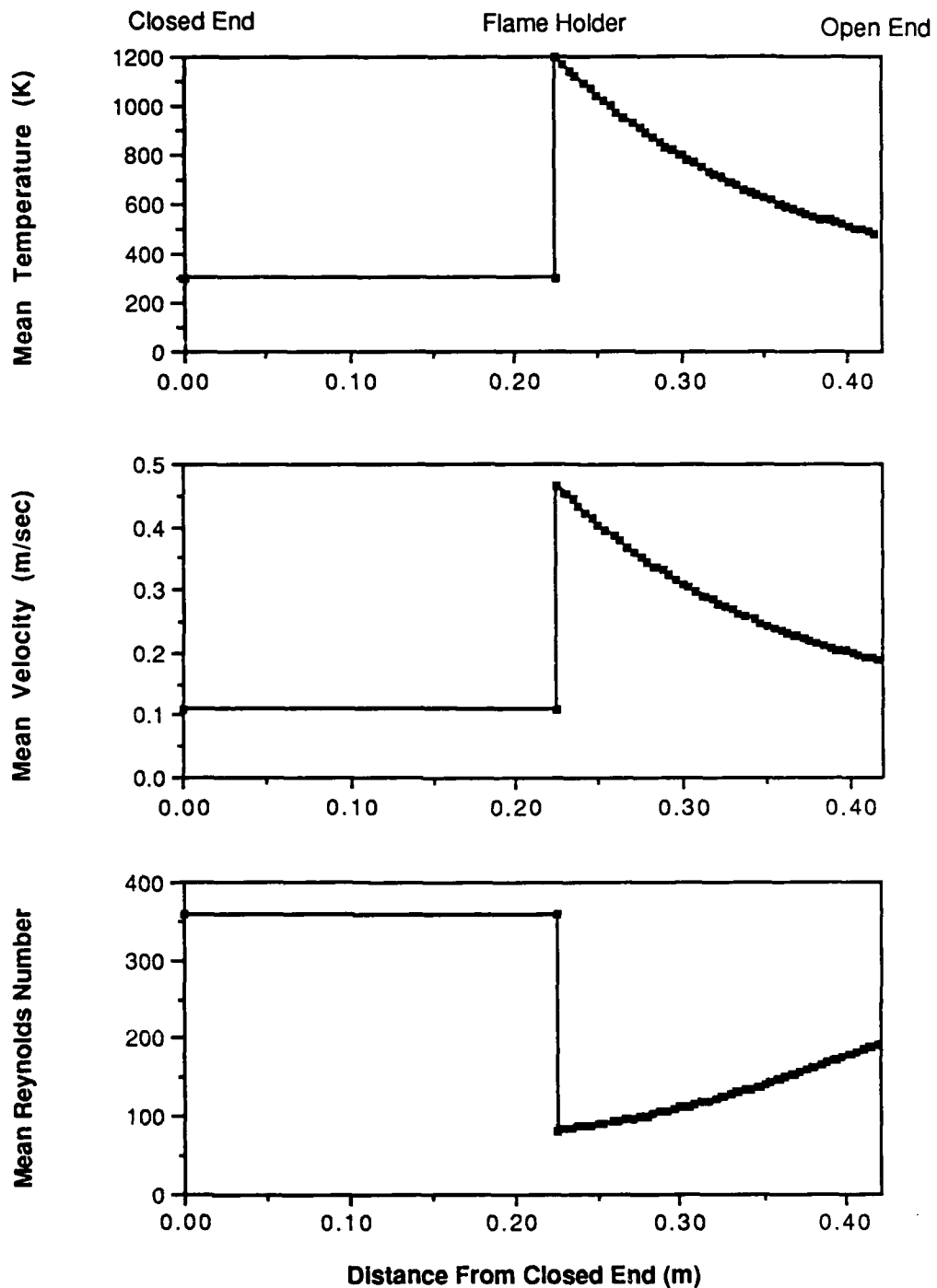
Figure 28. Mean temperature, velocity, and Reynolds number profiles along the burner as predicted by RIJKE.FOR.

5.2 Oscillating Gas Property Prediction

The oscillating property equations (i.e. acoustic equations) were derived by Raun from mass, momentum, and energy equations by linear perturbation analysis.

To predict the correct acoustic growth rates required modeling the acoustic flame interactions. Selecting the boundary conditions at the flame is the most critical part of modeling the acoustic-flame interactions in a burner. Across the flame interface, the acoustic pressure is constant, but the acoustic velocity has a discontinuity. Raun (1985) derived the following modified Bailey equation to describe the relationship between the acoustic velocity on the upstream and downstream side of the flame interface:

$$\hat{u}_2 = \left[\frac{\Lambda\delta^2 + 1 - (\Lambda + 1)\delta\omega\tau + (\omega\tau)^2 - i\delta(\Lambda - 1)}{(\delta - \omega\tau)^2 + 1} \right] \hat{u}_1$$

where

$\hat{u}_2$ is the oscillating velocity on the hot side of the flame interface (m/sec),

Λ is the ratio of upstream density to downstream density (ρ_1/ρ_2),

δ is σ/ω (1/sec),

$\sigma = du_f/d\varepsilon$, a positive constant which is the derivative of the flame speed with respect to distance from the flame holder (1/sec),

u_f = the steady state flame speed (m/sec),

ε is the distance between the flame and the flame holder (m),

ω is the complex frequency (radians),

τ is the characteristic time lag (sec),

i is the imaginary number, square root of -1,

$\hat{u}_1$ is the oscillating velocity on the cold side of the flame interface (m/sec).

Using this model the values of the flame parameters, τ and σ, must be known to calculate an acoustic growth rate. Approximate values of the flame parameters were estimated from the literature. As shown by Burcat[48] and Jachimowski[49] the time lag is very sensitive to the flame temperature and increases as the flame temperature decreases. A theoretical value of the ignition delay time at atmospheric pressure for a stoichiometric propane-air flame can be estimated from Figure 29. For a flame temperature of 1200K, an ignition delay time of 3 msec is predicted and for a temperature of 1000K, a delay time of 40 msec is predicted. However, the gas mixture used in the variable cool length data set had a $O_2/(N_2 + O_2)$ mass ratio of 0.232, which is higher than the 0.21 value naturally occurring in air. Consequently, the time lag would be expected to decrease because less nitrogen is present to absorb energy. A theoretical value for σ is much more difficult to determine. Bailey[36] proposed that the physical value of σ, which describes how the flame speed changes with respect to the distance from the flame holder, is likely affected by a heat transfer, chemical, or aerodynamic effect of the holder. His maximum experimental value was approximately 750 sec^{-1}. However, his model did not include a time lag term, a higher value of σ was required in this work.
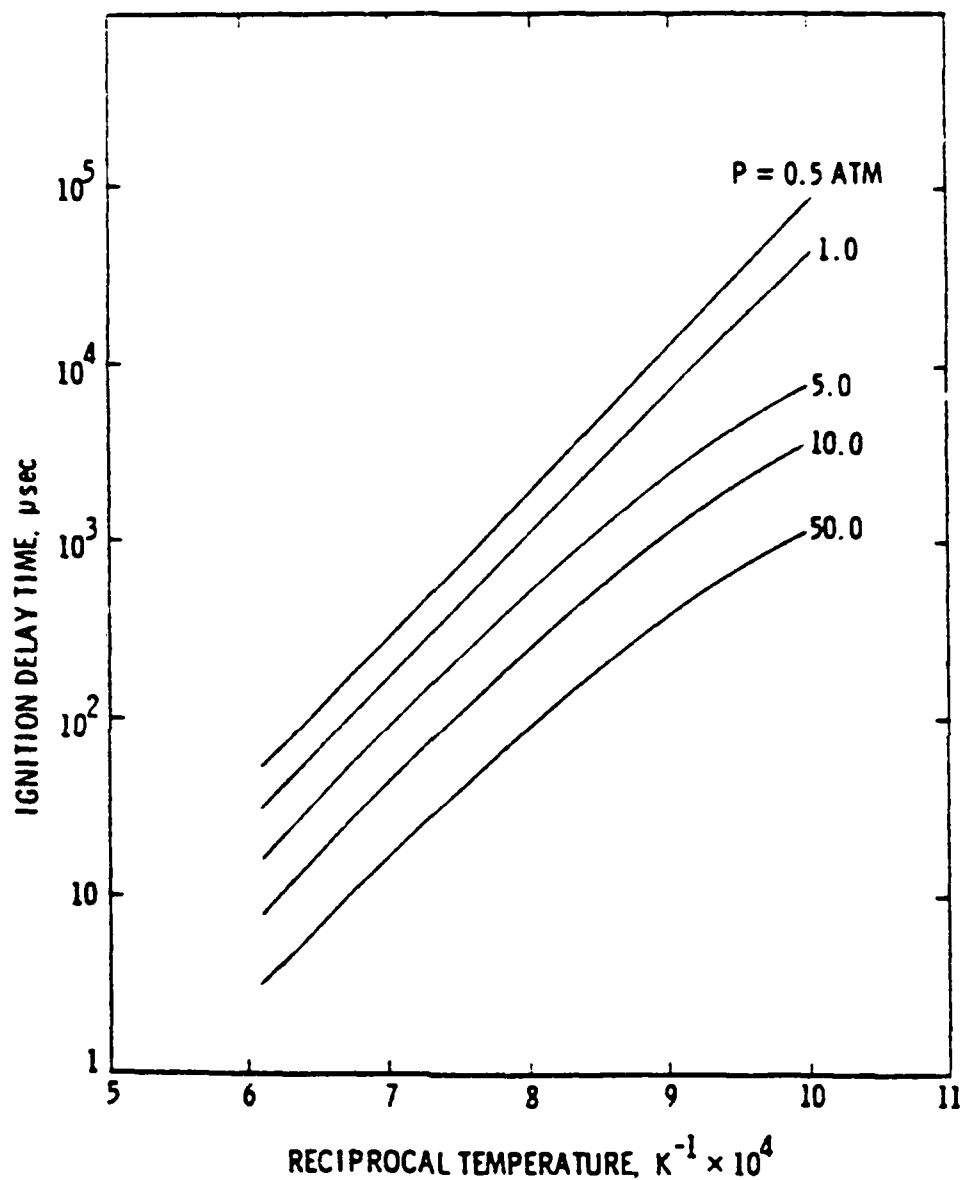
Figure 29.   Ignition times as a function of temperature and pressure for a stoichiometric propane-air mixture.

Calculations were made for cool section lengths of 225, 260, and 350 mm varying the value of τ from 10^{-2} to 10^{-6} and the value of σ from 1000 to 5000[50].   The results show that σ influences the amplitude of the response and τ shifts the peak of the first four modes.   For a cool section length of 350 mm, σ must be greater than approximately 1500 to achieve the alpha of 270 required to match the experimental data.

The flame parameters were adjusted to achieve an α of 270 in the second mode, using a cool section length of 350 mm, a hot section length of 180 mm, and a frequency of 830. Parameter values of $\tau = 0.63$ msec and $\sigma = 3500$ resulted in the desired α in the second mode with significantly smaller values of α in the other modes. Using these values of τ and σ, the acoustic growth rates for the first 4 modes were predicted while the cool section length was varied from 100 to 600 mm. A plot of the predicted acoustic growth rates as a function of cool section length for the first 4 modes is shown in Figure 30. The fundamental mode is stable except for cool section lengths less than 150 mm. For lengths of 100 to 250 mm, the first mode is predicted to be predominant, and for lengths of 250 to 500 mm, the second mode is predominant. The third mode becomes important as the length increases further.

In Figure 31 the predicted growth rates are compared with experimental data (Figure 21) for the lengths of 200 to 450 mm.

Figure 30. Predicted acoustic growth rates for the first 4 modes vs cool section length.
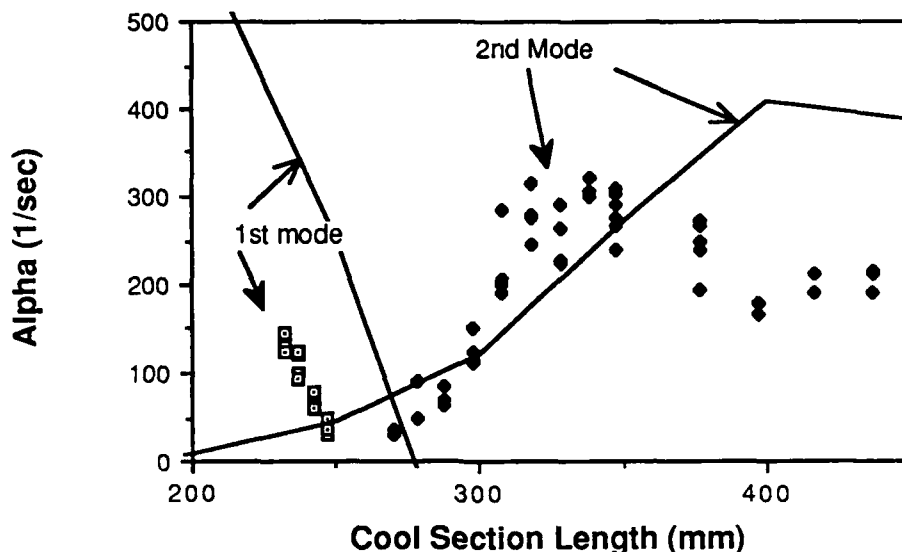
Figure 31. Comparison of the calculated growth rates (lines) with the experimental values (points) for the variable cool section data set as a function of cool section length.

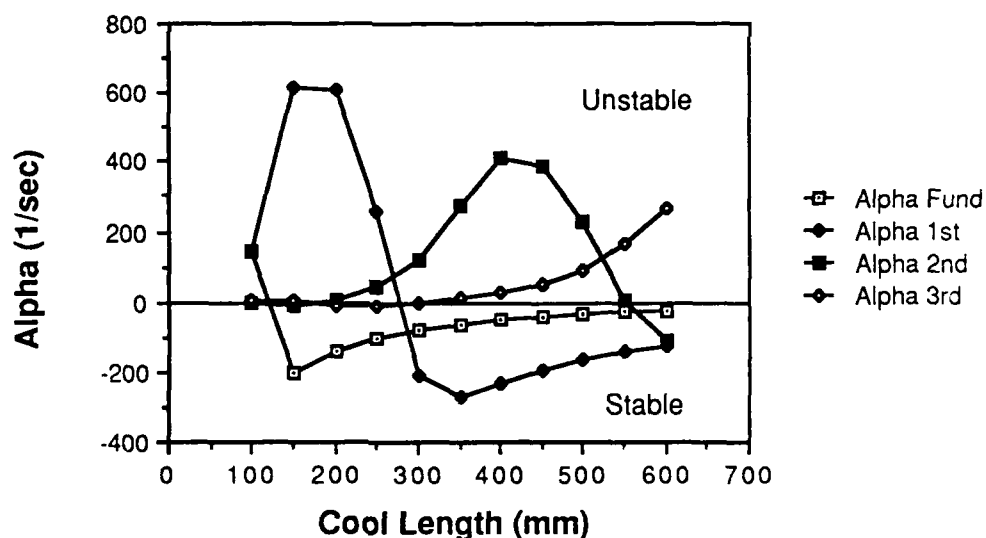Although the predicted growth rates, shown by the solid lines, vary slightly from experimental points, the trend of the first and second mode are correctly predicted. As the cool section length increases from 250 to 300 mm the second mode becomes dominant. The excellent qualitative nature of the fit gives increased confidence in using the RIJKE model to interpret Rijke burner data. By using an optimization routine to adjust the values of τ and σ, the fit could probably be improved significantly.

Figure 32 shows the calculated pressure, velocity, and pressure times velocity (PxV) mode shapes for the first four modes at a cool section length of 225 mm. Note that the acoustic pressure is continuous, but the acoustic velocity has a discontinuity at the flame interface. According to the Rayleigh Criterion, the product of pressure times velocity (PxV) can be used to investigate the stability of the respective modes. At the flame interface PxV for the fundamental mode is negative indicating its stability. Since the first mode has the highest normalized value of PxV at the flame, it would be expected to be the most unstable. The second mode would be predicted to be only slightly unstable, while both the fundamental and the third mode are predicted to be stable. Naturally, the predictions agreed with experimental data, since they were fit using experimental data.

The pressure times velocity curves from Figure 32 are summarized in Figure 33a. Figure 33a shows that for a cool length of 225 mm the PxV product is much larger at the flame, which indicates why the first mode is highly unstable. The second mode is only slightly unstable and the fundamental and third modes are stable. Figure 33b shows that for a cool length of 350 mm the second mode is the most unstable followed by the 3rd mode. The fundamental and 1st modes are both stable.

50

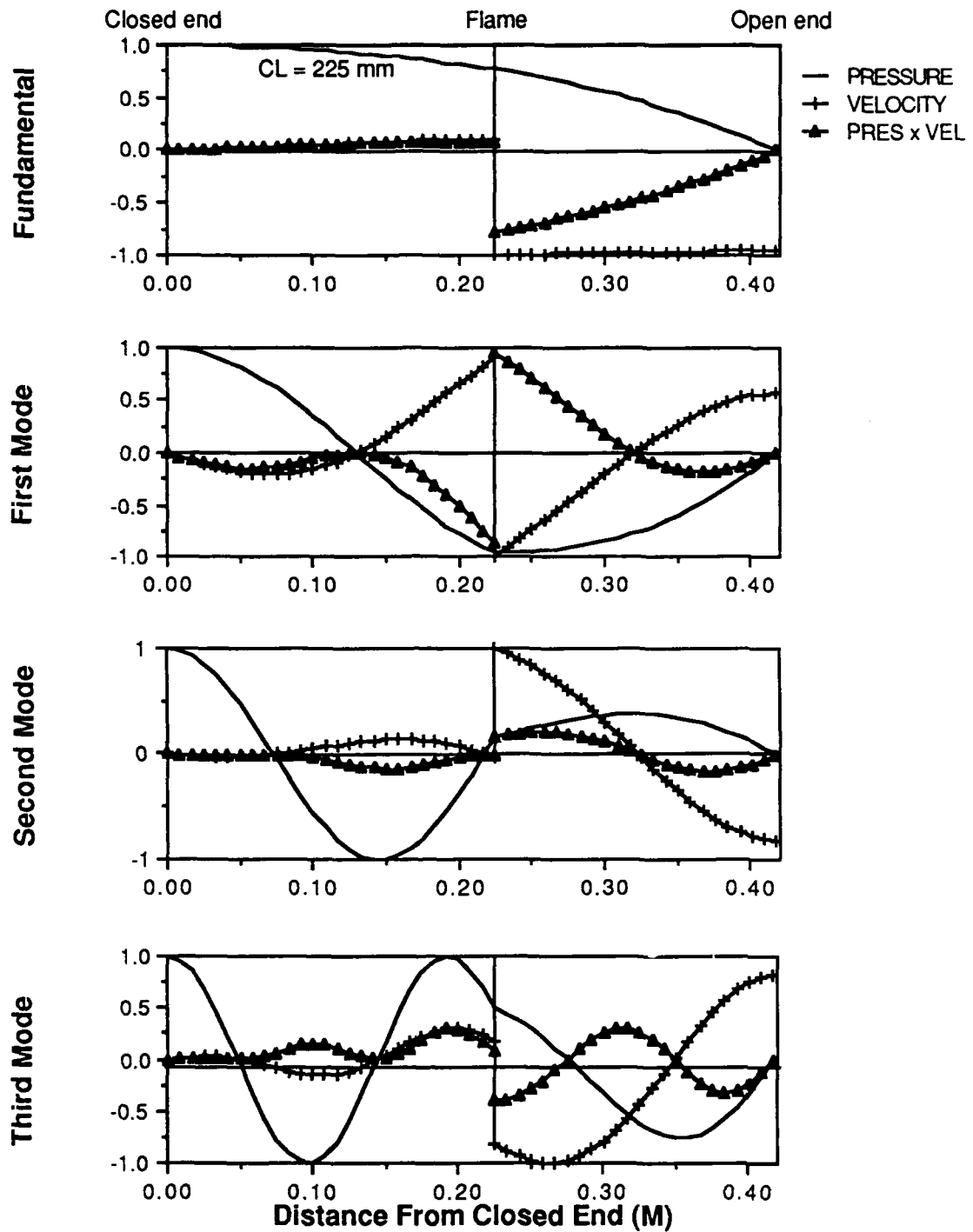Figure 32. Calculated pressure, velocity, and pressure times velocity (PxV) mode shapes for the first four modes at a cool section length of 225 mm, τ = 0.63 msec and σ = 3500.
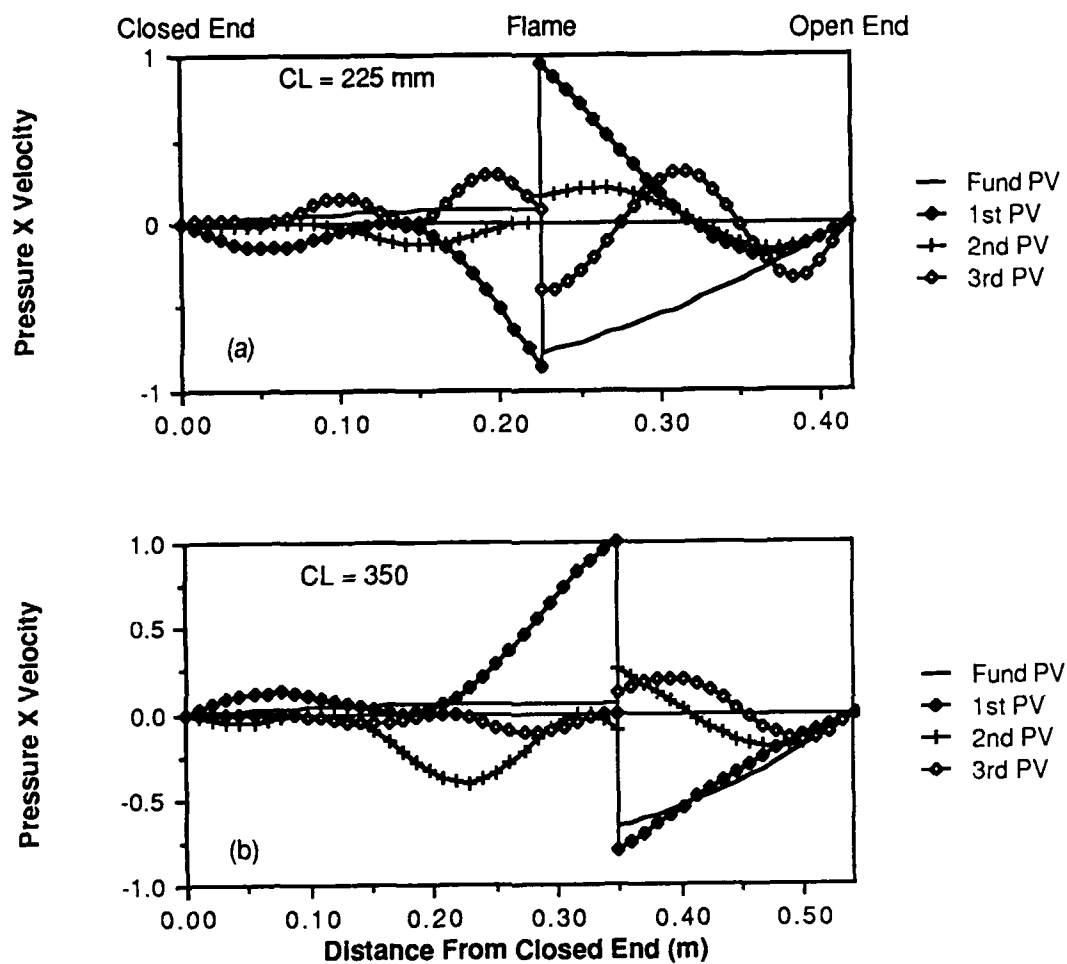
Figure 33 a,b. Calculated pressure times velocity (PxV) mode shapes for the first four modes at cool section lengths of 225, and 350 mm, $\tau = 0.63$ msec and $\sigma = 3500$.

5.3 Comparison of RIJKE Model With Experimental Data

Several different approaches have been attempted to fit the Rijke burner experimental data discussed in Section 3.4.1 with the RIJKE model. Each approach has required a method of determining the flame parameters, σ and τ, of the Bailey model. These approaches are summarized below including difficulties encountered and problems resolved.

Stoichiometric Variation: Figure 19 in Section 3.4.1 is a graph of the experimental data based on constant total mass flowrates at varied stoichiometric ratios. Several approaches were used to match these data with the model. The first was to use constant values of σ =3500 and τ =0.63x10^{-3} as discussed in the previous section. These parameter settings only gave a very slight variance in alpha, but not corresponding to the variation observed in the experimental data. Utilization of a constant τ does not give the desired characteristics, probably due to the fact that τ is dependent on temperature and there is a variation in flame temperature due to the variation in stoichiometry.

A second approach was to utilize data from the shock tube study by Burcat, et.al.[48] to account for the variation of τ due to temperature. Because Burcat did not use the same concentrations of fuel and oxygen as above, the τ vs temperature plots were first shifted linearly according to the ratio of fuel concentrations. The flame temperatures were obtained using the adiabatic flame temperatures calculated by the Edwards thermochemical code, and then decreased by accounting for the heat loss to the cooling water. In order for these new values of τ to allow the model to fit the experimental data, σ also had to be varied. The range of σ and τ were 368 to 2911 and 0.010x10^{-3} to 0.019x10^{-3}, respectively, in order to fit the data, with the growth rate increasing with total mass flow rate as observed.

A better approach for obtaining τ was then used taking into account the mechanism of the reaction as studied by Burcat, et.al. This relationship is as follows:

$$\tau \, [O2]^{1.22}[C3H8]^{-0.57} = 4.4 \times 10^{-14} \exp(42200/RT)(s.mol/cm^3)^{0.65}$$

where $C_i = x_i P/RT$, $P=0.83$ atm, R is the gas constant, and T is the estimated flame temperature. This approach allows τ to vary with reactant concentration and gas temperature, which is a more realistic approach. The range of σ and τ values required to fit the data were 640 to 2114 and 0.073x10^{-3} to 0.147x10^{-3}, respectively. Using this approach the trends in the data were matched quite precisely.

Cold Length Variation: Figure 21 in Section 3.4.1 is a graph of the experimental data based on constant gas flowrates for varying cold length. For the model to match these data, as discussed in the previous section, σ and τ were arbitrarily varied in the

range 1000 to 5000 and 10^{-6} to 10^{-3}, respectively, until a curve of similar trends was obtained. The values obtained were σ =3500 and τ =0.63x10^{-3}. The alpha vs cold length graphs for these values was presented in Figures 30 and 31, and discussed in the previous section.

An alternative approach was to use an optimization computer code with selected cold length setpoints (based on experimental data) and minimize the sum of the squares of the differences between the calculated values and the selected data points. The optimized parameter values obtained were σ =1134 and τ =0.208x10^{-3}. The alpha vs cold length graph for these values is shown in Figure 34 with the actual data plotted for comparison. The improvement in the calculated values over the results in Figures 30 and 31 is apparent, but still less than desirable.
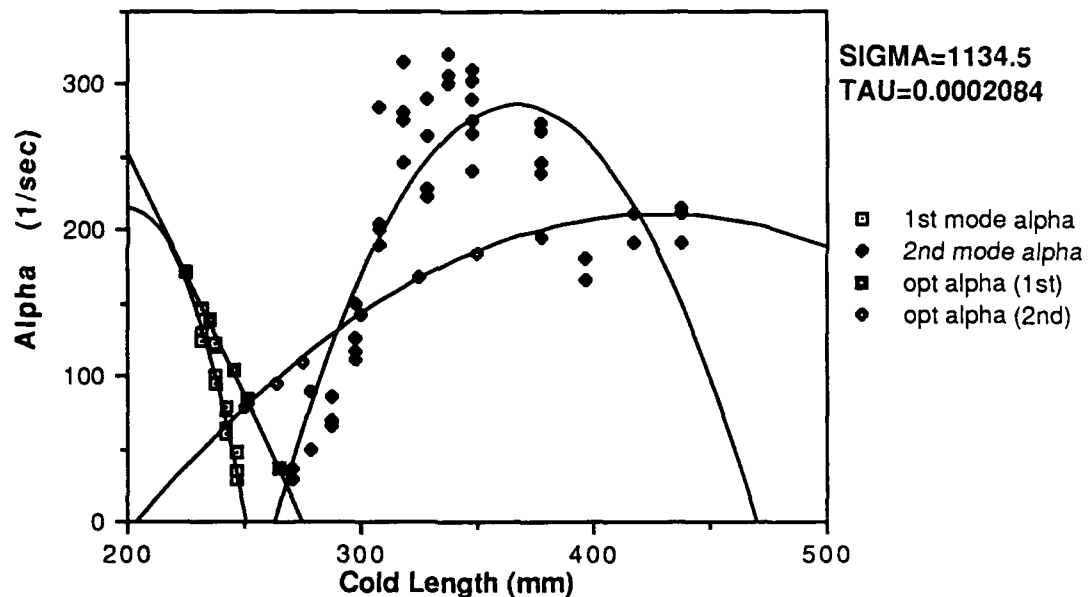
Figure 34. Comparison of calculated and measured growth rates for the Rijke burner with optimized values of σ and τ.

A third approach was to calculate τ based on the above noted relationship by Burcat[48]. For the experimental flowrates and the estimated flame temperature, τ should have a value of 0.274 msec. Using the optimization approach described above yields a value of σ =1350. The alpha vs cold length graph for these parameter values is shown in Figure 35, which is not significantly different from the results of Figure 34.
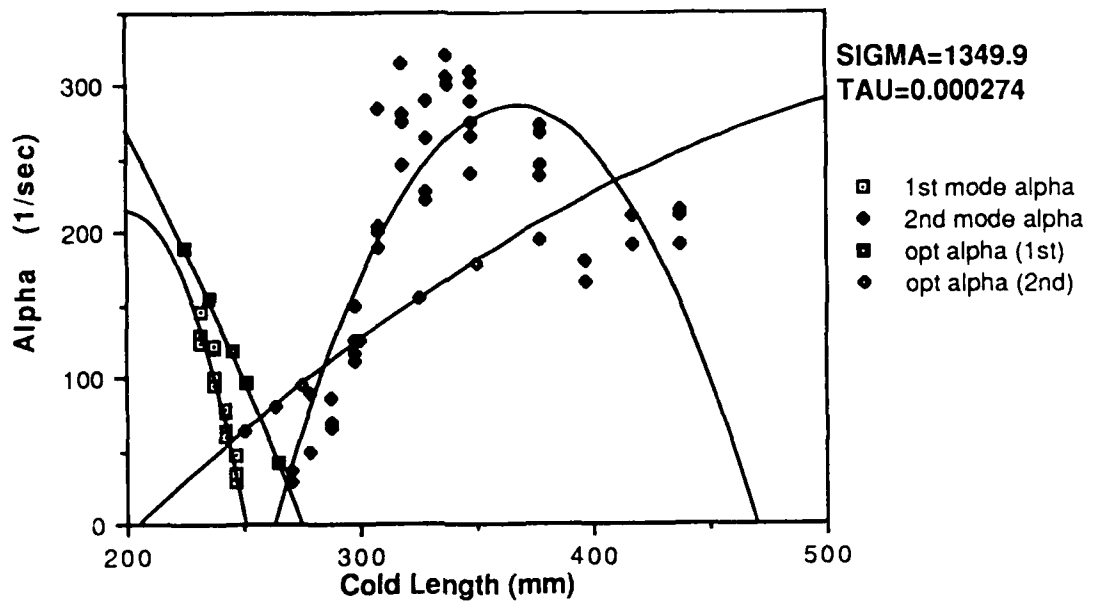
Figure 35.   Comparison of calculated and measured growth rates for the first two modes in the Rijke burner with τ determined from the Burcat[48] correlation and σ optimized.

It is apparent from the results of Figures 34 and 35 that an optimum value of τ is on the order of 0.2 to 0.3 msec and σ is ~ 1.1 to 1.3 msec^{-1}, whichever approach is taken. Time constants of approximately one millisecond do not appear to be unrealistic for the propane air flame.

6.0 SUMMARY AND CONCLUSIONS

This report summarizes the work performed on a research program to study the acoustic interaction of particle additives used in solid propellants for performance enhancement and acoustic suppression. A modified Rijke burner which had been constructed previously has been modified extensively and characterized to aid in the study. The report discusses various examples found in the literature that give evidence to the existence and nature of distributed combustion. The basic approach used with the Rijke burner has been discussed, and a brief description of the mathematical model presented. The results from the model have been compared with the experimental data.

Distributed combustion refers to a burning particle which reacts far from the burning surface, exchanging energy with an acoustic environment. This process has generally been ignored in acoustic analyses of rocket motors in the past. A variety of literature sources have been examined for evidence of distributed combustion, and are documented in this report. Velocity coupled T-burners indicate response functions of ~10 for metallized propellants, while non-metallized propellants typically have measured response functions of ~1. The large response function is apparently due to distributed combustion of burning metal rather than velocity coupling. In addition, velocity coupled T-burner data give response functions varying with test sample location, which is inconsistent unless the observed effect is due to distributed combustion. Attempts have been made to measure velocity coupling using end vented burners, but again, inconsistent answers result, indicating an effect of distributed combustion. Pulsed/decay T-Burners usually measure different particle damping than variable area T-Burners with metallized propellants. Also, some T-burner data show the combustion growth rate varying with aluminum particle size, indicating a distributed combustion effect due to the burning aluminum. Furthermore, specific calculations indicate large burning times for burning Al agglomerates compared to T-burner residence times. These combined results indicate that distributed combustion may well be the cause for many previously unexplained observations of combustion instability.

The Rijke burner has been modified and developed as a tool to study oscillatory and distributed combustion. To validate the theoretical model and to better understand the modified Rijke burner, the burner was characterized without the addition of particles. The acoustic growth rate of the burner has been characterized experimentally as a function of frequency, flame position, length, inlet gas compositions (O_2, N_2, C_3H_8), and energy balance. Stability boundaries have been determined as a function of the fuel/air ratio. Growth rates were observed to increase with increasing oxygen content and overall mass flow rate. Often, minor changes in test conditions would result in changes of oscillating mode. Increasing the cold length of the burner caused a decrease in the first mode growth rate, an increase in the second mode growth rate and a maximum in that growth rate. The data indicate that the overall acoustic driving forces in a Rijke burner are dependent upon the acoustic mode shape relative to the flame location and the distribution of energy through the burner, (i.e. the gas flow rates and heat losses). By changing the burner length or

reducing the net energy density by the addition of inert gases, the flame apparently shifts from a position of maximum driving and the acoustic growth rate is reduced.

A mathematical model for the Rijke burner has been developed which accounts for the effects of heat loss, variable gas temperature, and particle interactions on acoustic oscillations. The model has been verified by comparing predicted frequency and growth rates for several simple test cases with the corresponding analytical solutions. Initially acoustic response of the Rijke burner flame was approximated using simple flame models originally developed by Merk and by Bailey. These models do a fair job of predicting acoustic growth rate when heat loss is taken into account. However, to describe the acoustic mode shape accurately, temperature variation must be taken into account. Models which assume a constant gas temperature, such as those of Merk and Bailey, will not predict the correct mode shape, and cannot be used. The Merk and Bailey models also assume that the flame responds instantaneously to acoustic oscillations. An extension of the Merk and Bailey models has been developed, allowing the flame to have a first order time lag, making the flame model a two parameter model. Experimentally-measured frequency and growth rate can be matched exactly by adjusting the two parameters in this model.

The variable cold length data set was selected as a standard experimental data set for verification of the model. It was selected because the flame parameters should be constant for the entire data set, and the oscillations were observed to change from first to second mode as the burner length changed, which gives a severe test to the model. Within the model the dimensions, flow rates, and temperatures of the burner were fixed, and the flame parameters, τ and σ, were adjusted to fit the variable cold length data set. Initially parametric studies were performed showing that τ and σ values on the order of 0.6 msec and 3.5 msec^{-1}, respectively, were required to fit the data. These values appear to be physically realistic. Literature data on the ignition of propane in air were also used to evaluate the time constant, τ. Using an optimization program to compare the model to the data resulted in values of τ and σ between 0.2 and 0.3 msec and 1.1 and 1.3 msec^{-1}. These gave excellent results in comparison with the actual data. Using the model to make the comparison with the data provides insight into the acoustic oscillations that is difficult to achieve by other methods of analysis.

7.0 NOMENCLATURE

B	parameter in Equation (5).
c	speed of sound in gas, m/sec.
C_p	constant pressure heat capacity, J/kg-K.
C_{pgi}	heat capacity of gas species i, J/kg-K.
f_{pj}	aerodynamic force on particle class j, N/m^3.
g	acceleration of gravity, m/sec^2.
h	enthalpy per unit mass, J/kg.
h_{gi}	partial mass enthalpy of gas species i, J/kg.
h_g	enthalpy of bulk gas, J/kg.
h_{sj}	enthalpy of material which has just left particle surface due to reaction, J/kg.
i	$\sqrt{-1}$.
p	gas pressure, Pa.
q_{cpj}	rate of heat transfer from gas to particles, J/m^3-sec.
g_{sg}	rate of heat loss from gas to surroundings, J/m^3-sec.
R	radius of Rijke burner, m.
r_{gi}	reaction rate of ith gas species, kg/m^3-sec.
r_{pj}	reaction rate of particle class j, kg/m^3-sec.
t	*time, sec.*
T	absolute temperature, K.
u	component of velocity in x direction, m/sec.
u_i	one-dimensional interface velocity, m/sec.
x	axial coordinate, m.

Greek symbols

α	initial growth rate, sec-1.
γ	ratio of specific heats.
δ	parameter in equations (6) and (7).
Λ	ratio of mean densities in cold and hot tube sections.
σ	derivative of flame speed to distance from gauze in equations (6) and (7).
τ	time lag.
ϕ	represents any general property.
ω	complex frequency = $\omega_0 - i\alpha$, sec-1.
ω_0	real circular frequency, sec-1.

Superscripts

$(\hat{\ })$	fluctuating property with $\exp(i\omega t)$ factored out.
$(\bar{\ })$	mean property.
$(\ )'$	fluctuating property with time dependency.
1	cold section property.
2	hot section property.
g	gas property.
i	interface; ith gas species.
j	jth particle class.
p	particle property.
s	surroundings.

8.0 REFERENCES

1. Beckstead, M.W., and Butcher, A.G., "The Velocity Coupled T-Burner", AIAA Paper 74-200, (1974); see also, Beckstead, M.W., Peterson, N.L., Butcher, A.G., and Horton, M.D., "A Technique for Evaluating Velocity Coupled Combustion Instability", 10th JANNAF Combustion Meeting, Vol II, CPIA No 243, (1973), pp 179-192.

2. Brown, R.S. Blackner, A.M., Willoughby, P.G., and Dunlap, R., "Coupling Between Acoustic Velocity Oscillations and Solid-Propellant Combustion", J. of Propulsion and Power, Vol 2, No 5, (1986), pp 428-437.

3. Brown, R.S., Waugh, R.C., Willoughby, P.G., and Dunlap, R., "Coupling Between Velocity Oscillation and Solid Propellant Combustion", 19th JANNAF Combustion Meeting, Vol I, CPIA No 366, (1982), pp 191-208.

4. Hercules, Inc., unpublished data, 1974.

5. Beckstead, M.W., Krashin, M., Butcher, A.G., and Pilcher, D.L., "Acoustic Stability Characterization of the Trident I (C4) Motors," 11th JANNAF Combustion Meeting, Vol I, CPIA No 260 (1974) pp. 535-566.

6. Butcher, A.G., and Beckstead, M.W., "The Effect of Propellant Type on Combustion Response Functions", 16th JANNAF Combustion Meeting, Vol III, CPIA No 308, (1979), pp 527-558.

7. Micheli, P.L., "Status of Velocity Coupling", 13th JANNAF Combustion Meeting, Vol II, CPIA No 281, (1976), pp 71-94.

8. Culick, F.E.C., "Stability of Longitudinal Oscillations with Pressure and Velocity Coupling in a Solid Propellant Rocket", Combustion Science and Technology, Vol 2, (1970), pp 179-201.

9. Beckstead, M.W., and Jensen, R.C., "Nonlinear Interpretation of Linear T-Burner Data", 9th JANNAF Combustion Meeting, Vol I, CPIA No 231, (1972), pp 239-248; see also, Jensen, R.C., and Beckstead, M.W., "Nonlinear Analysis of Combustion Instability Data", 10th JANNAF Combustion Meeting, Vol II, CPIA No 243, (1973), pp 163-177.

10. Beckstead, M.W., "Nonlinear Mechanisms of Solid Propellant Combustion Instability," 24th JANNAF Combustion Meeting, CPIA No 476, Vol , (1987) pp27-40.

11. Beckstead, M.W. et al., "Variable Area T-Burner Investigation," AFRPL-TR-72-85, Dec. 1972.

12. Micheli, P.L., "Evaluation of Pulsed T-Burner for Metallized Propellants," AFRPL-TR-72-54, Sept. 1973.

13. Derr, R.L., "Evaluation of a Variable Area T-Burner for Metallized Propellants," AFRPL-TR-72-97, Feb. 1973.

14. Peterson, J.A., Mihlfeith, C.M., and Sayer, L.H., "Pressure Oscillation Investigation for Minuteman III," AFRPL-TR-72-98, Jan. 1973.

15. Crump, J.E. et al., "Oscillatory Combustion Experimentation and Analysis Work in Support of an Air Force Program," Naval Weapons Center, Rept. NWC TP 5630 (AFRPL-TR-73-108), June 1974.

16. Mathes, H.B., Kraeutle, K.J., and Atwood, A.I., "Effect of Propellant Surface Orientation on the Combustion and Damping Behavior of Aluminized Propellants", 14th JANNAF Combustion Meeting, Vol I, CPIA No 292, (1977), pp 11-26; see also, Derr, R.L., Mathes, H.B., and Crump, J.E., "Pressure-Coupled Combustion Response Associated with End- and Side-Burning Samples in a T-Burner", 12th JANNAF Combustion Meeting, Vol II, CPIA No 273, (1975), pp 99-110.

17. Beckstead, M.W., Richards, R.S., and Brewster, B.S., "Distributed Combustion Effects on Particle Damping," AIAA J, Vol 22, No. 3, (1984) pp. 383-

18. Wendelken, C.P., Weiss, R.R., and Chew, T.J.C., "Combustion Instability Characteristics of Several Solid Rocket Propellants for Booster and Tactical Rocket Applications", 9th JANNAF Combustion Meeting, Vol I, CPIA No 231, (1972), pp 249-264.

19. Beckstead, M.W., Horton, M.D., Krashin, M. and Butcher, A.G., "Velocity Coupling Combustion Instability," AFRPL-TR-73-73, Hercules, Inc., (1973).

20. Beckstead, M. W., Braithewaite, P. C., and Gordon, D. L. "Measurements of Distributed Combustion",66th AGARD Meeting on Smokeless Propellants, Italy, Sept. 1985.

21. Stone, W.C. "Workshop Report: Acoustic Instability in a High Burning Rate-High Pressure Regime," 21st JANNAF Combustion Meeting, Vol. II, CPIA No 412, (1984) pp 113-118.

22. Raun, R. L., "A Numerical Model of the Rijke Burner," Ph.D. Dissertation, Brigham Young University, Provo, Utah. (1986)

23. Joos, F. and Vortmeyer, D., "Self-Excited Oscillations in Combustion Chambers with Premixed Flames and Several Frequencies," Combustion and Flame, Vol. 65, pg. 253, (1986)

24. Seto, W. W., Schaum's Outline Series - Theory and Problems of Acoustics, Mc-Graw Hill Book Company, New York, New York, p. 56. (1971)

25. Feldman, K. T. Jr., "Review of the Literature on Rijke Thermoacoustic Phenomena " Journal of Sound and Vibration, Vol. 7, No. 1, pg 83 (1968).

26. Kinsler, L. E. , et. al. *Fundamentals of Acoustics,* Third Edition, John - Wiley & Sons, Inc., New York, p. 156. (1982)

27. Diederichsen, J., "A Singing Flame as a Tool for Evaluation of Damping Agents for Solid Propellant Rocket Motors," *Combustion and Flame,* Vol. 7, (Mar. 1963).

28. Braithewaite, P.C., "Measurements of Distributed Combustion in the Rijke Burner," M.S. Thesis, Brigham Young University, (1984).

29. Nickerson, G. R., "Standard Stability Prediction Method for Solid Rocket Motors", AFRPL TR-83-017, (Sept 1983)

30. Borse, G.J., *FORTRAN 77 and Numerical Methods for Engineers,* PWS Engineering, Boston (1985).

31. Davis, M. E., *Numerical Methods and Modeling for Chemical Engineers,* John Wiley & Sons, New York (1984).

32. Glassman, I., *Combustion,* chapter 1, Academic Press, New York, (1977).

33. Hanby, V. I., "Convective Heat Transfer in a Gas-Fired Pulsating Combustor," *Journal of Engineering for Power,* pg 48, (January 1969).

34. Neuringer, J. L. and Hudson, G. E., "An Investigation of Sound Vibrations in a Tube Containing a Heat Source," *The Journal of the Acoustical Society of America,* Vol. 24, No. 6, (1952), pp. 667-674.

35. Carrier, G.F., "The Mechanics of the Rijke Tube," *Quarterly of Applied Mathematics,* Vol. 12, No. 4, (1954), pp. 383-395.

36. Bailey, J.J., "A Type of Flame-Excited Oscillation in a Tube," *Journal of Applied Mechanics,* Vol. 24, No. 3, (September 1957), pp. 333-339.

37. Jones, H., "The Mechanics of Vibrating Flames in Tubes," *Proceedings of the Royal Society of London, Series A,* Vol. 353, (1977), pp. 459-473.

38. Jones, H., "The Generation of Sound by Flames," *Proceedings of the Royal Society of London, Series A,* Vol. 367, (1979), pp. 291-309.

39. Mugridge, B.D., "Combustion Drive Oscillations," Journal of Sound and Vibration, Vol. 70, No. 3, (1980), pp. 437-452.

40. Crowe, C. T., and Smoot, L.D., "Multicomponent Conservation Equations," *Pulverized-coal Combustion and Gasification Theory and Applications for Continuous Flow Processes,* L. Douglas Smoot and David T. Pratt, editors, Plenum press, New York, NY, (1979), pp. 15-54.

41. Williams, F.A., <u>Combustion Theory</u>, Addison-Wesley Publishing Company, Reading, MS, (1965) p. 14.

42. Hornbeck, R.W., <u>Numerical Methods</u>, Quantum Publishers, Inc., New York, NY, (1975).

43. Temkin, S. and Dobbins, R.A., "Attenuation and Dispersion of Sound by Particulate-Relaxation Processes," <u>The Journal of the Acoustical Society of America</u>, Vol. 40, No. 2, (1966), pp. 317-324.

44. Culick, F.E.C., editor, "T-burner Testing of Metallized Solid Propellants, Final Report," Air Force Rocket Propulsion Laboratory Report AFRPL-TR-74-28, (October, 1974), pp. 213-217.

45. Merk, H.J., "Analysis of Heat-driven Oscillations of Gas Flows: I. General Considerations," <u>Applied Scientific Research</u>, Vol. A6, (1956-57a), p. 317.

46. Merk, H.J., "Analysis of Heat-driven Oscillations of Gas Flows: II. On the Mechanism of the Rijke-tube Phenomenon," <u>Applied Scientific Research</u>, Vol. A6, (1956-57b), p. 402.

47. Merk, H.J., "An Analysis of Unstable Combustion of Premixed Gases," <u>Sixth Symposium (International) on Combustion</u>, Reinhold, New York, NY, (1957), pp. 500-512.

48. Burcat, A., Lifshitz, A., Scheller, K., and Skinner, G. B., " Shock-tube Investigation of Ignition in Propane-Oxygen-Argon Mixtures", <u>Thirteenth Symposium (International) on Combustion</u>, The Combustion Institute, Pittsburg, Pa, (1971), pp. 745; see also, Burcat, A., Scheller, K., and Lifshitz, A., "Shock-Tube Investigation of Comparative Ignition Delay Times for C_1-C_5 Alkanes", <u>Combustion and Flame</u>, Vol. 16, (1971), pp. 29-33.

49. Jachimowski, C. J., "Chemical Kinetic Reaction Mechanism for the Combustion of Propane", <u>Combustion and Flame</u>, Vol. 55, 1984, pp. 213-224.

50. Finlinson, J.C., "Experimental Characterization of a Modified Rijke Burner," M.S. Thesis, Brigham Young University, (1988).